https://doi.org/10.5194/egusphere-2026-4406
Preprint. Discussion started: 4 September 2026

Carboniferous-Triassic rise and fall of continental arc recorded by retro-arc shifts of basin-infill and climate in the Hexi Corridor

Junxiang Zhang[1], **Jiaopeng Sun[1*]**, Yunpeng Dong[1], Xiaofeng Han[2], Xiangyang, Yang[3], Yukun Qi[1]

[1]State Key Laboratory of Continental Evolution and Early Life, Department of Geology, Northwest University, Xi'an 710069, China
[2]Xi'an Center of China Geological Survey/Northwest China Center for Geoscience Innovation, Xi'an 710119, China
[3]Department of Geotechnical Engineering, Chongqing Jiaotong University, Xuefu Str. 66, Chongqing 400074, China

Correspondence to:Jiaopeng Sun (sunjiaopeng@nwu.edu.cn)

Abstract

The Hexi Corridor inboard the Andean-type North China Continental Arc preserves pivotal records of basin transition and dynamic change in Carboniferous-Triassic. This work provides an integrated study on strata in the Eastern Hexi Corridor Belt (EHCB) and western Ordos. Provenance analyses show that Carboniferous strata in the southern EHCB were sourced from the Central Qilian, evidenced by north-direct paleoflow data and age profiles mainly of Paleozoic and Neoproterozoic clusters. The northern EHCB samples have age spectra with dominance of ca. 2700–1700 Ma ages, implying sources from the Ordos basement, which is compatible with south-direct paleoflow. Crustal thinning and mantle-derived magmatism indicate an extension setting for the EHCB. Shallow-water deposition in the EHCB was terminated at ca. 295 Ma. The late Permian strata were fed by the intensely raised Nuru-Langshan Continental Arc (NLCA), given occurrence of >80% number of Paleozoic-age zircons in forearc and retroarc samples. Crustal thickening and negative ε(Hf) values for plutons demonstrate raising of the NLCA, cratonward expansion of which constructed a retroarc foreland system in the western Ordos and EHCB. The ~3±0.5 km high relief of the IMCA triggered orographic rain shadow and retroarc aridification, expressed by changing of mudstone color from black to red. The Paleo-Asian Ocean closure at early Triassic induced uplift of the NLCA basement and left-lateral strike-slip of the Bayanwula Fault, providing a swath of zircons of ca. 2700–1700 Ma ages to the retroarc. Paleodrainage reorganized, as fluvial-delta systems in the western Ordos commenced routing to the southeast.

https://doi.org/10.5194/egusphere-2026-4406
Preprint. Discussion started: 4 September 2026

1 Introduction

Andean-type continental arcs form where oceanic lithosphere subducts beneath an overriding continental plate. They are important settings for studying mountain building, continental growth, and long-term climate evolution (DeCelles et al., 2009; Boschman, 2021; Garzanti et al., 2022; Ding and Lithgow-Bertelloni, 2025). Lithosphere-atmosphere carbon recycling and uplift-driven rain shadows can strongly influence Earth's climate through geological time (Mason et al., 2017; Plank and Manning, 2019; Song et al., 2023). For example, late Paleozoic glacial-deglacial cycles temporally overlap with tropical arc activity (McKenzie et al., 2016; Montanez, 2016; Wu et al., 2024). A detailed understanding of Andean-type continental-arc evolution is therefore essential for reconstructing past tectonic and climatic systems. However, arc histories are commonly difficult to resolve because magmatic reworking and structural destruction can obscure primary records (Cawood et al., 2012). Arc-related basins provide complementary stratigraphic archives that record mountain building, paleogeographic configuration, and drainage change along active continental margins (DeCelles et al., 2015; Terrizzano et al., 2017; Garzanti et al., 2022; Sundell et al., 2025).

The Central Asian Orogenic Belt (CAOB), the largest accretionary orogen on Earth, records the evolution and final closure of the Paleo-Asian Ocean (PAO), which played an important role in the assembly of northeastern Pangea (Jahn et al., 2004; Xiao et al., 2015, 2020; Sengor et al., 2018; Zhao et al., 2018; Song et al., 2018, 2024a). Southward subduction of PAO lithosphere generated a north-facing continental mountain belt extending from the North China Block (NCB) through Alxa to Tarim (Xiao et al., 2015; Song et al., 2020, 2021, 2024b). As part of this continental-arc system, thick Carboniferous-Triassic successions in the retroarc Eastern Hexi Corridor Belt (EHCB) provide a key archive of accretionary tectonics and the closure history of the southern CAOB (Sun and Dong, 2020; Sun et al., 2024). However, the evolution of this retroarc basin system remains less well constrained.

Here, we combine sedimentology, paleocurrent analysis, sandstone petrography, and detrital zircon U-Pb geochronology from Carboniferous-Triassic strata in the EHCB and western Ordos Basin. Our new data and observations show that sedimentary changes in the retroarc EHCB and western Ordos Basin closely tracked shifts in the tectonic regime of the continental arc. These results define an evolving Andean-type retroarc basin system during PAO closure and provide a basin-based perspective on continental-arc uplift and Paleo-Asian Ocean evolution.

https://doi.org/10.5194/egusphere-2026-4406
Preprint. Discussion started: 4 September 2026

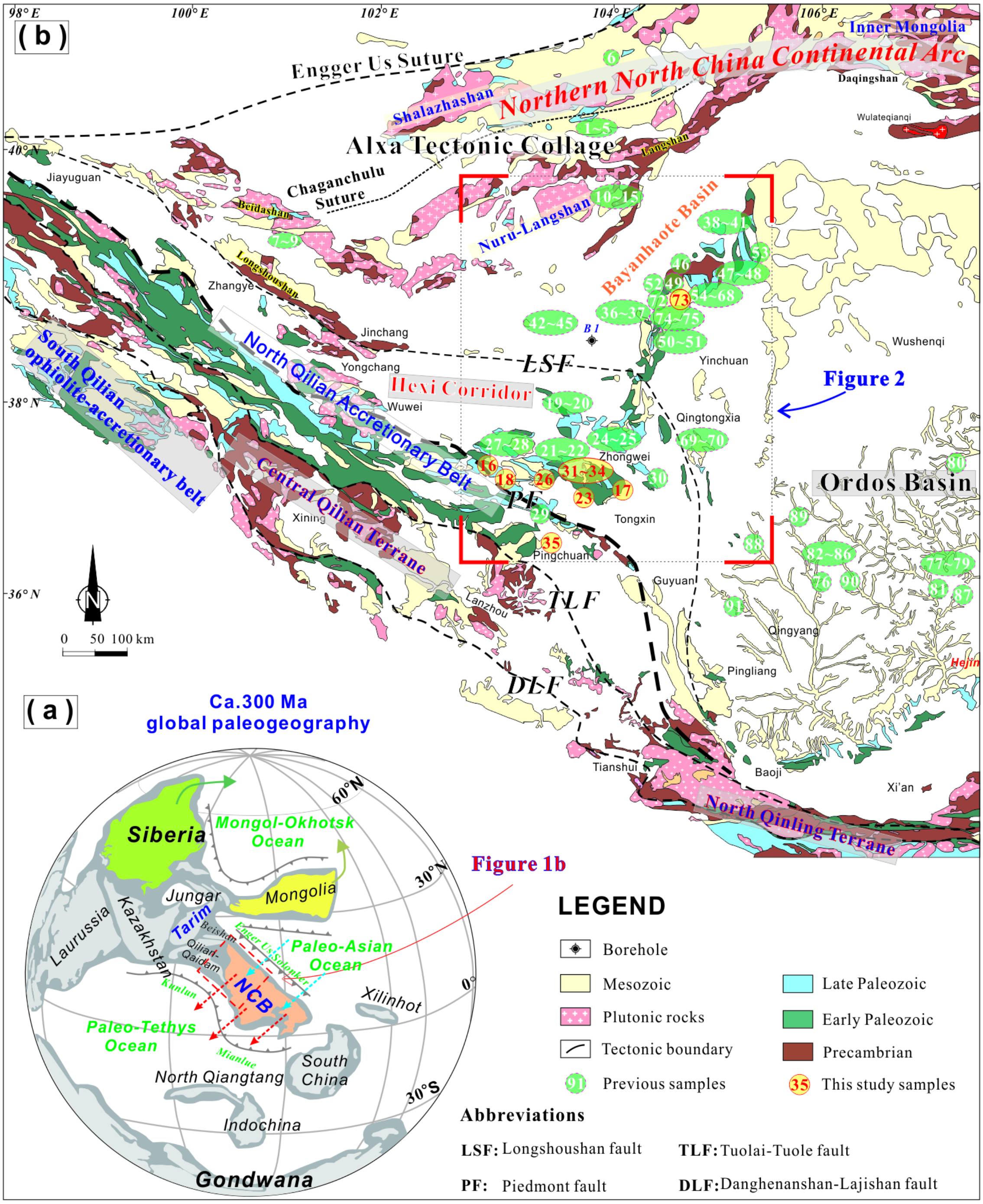

Figure 1. Geological settings of the study area. (a) The geographic reconstruction of Central Asia at ca. 300 Ma (modified from Liu et al., 2024) and moisture direction (Tabor and Poulsen, 2008) (b) Tectonic overview of the Hexi Corridor tectonic belt and adjacent geologic units (modified from Sun and Dong, 2024). See references for all samples in Supplementary Table 1.

https://doi.org/10.5194/egusphere-2026-4406
Preprint. Discussion started: 4 September 2026

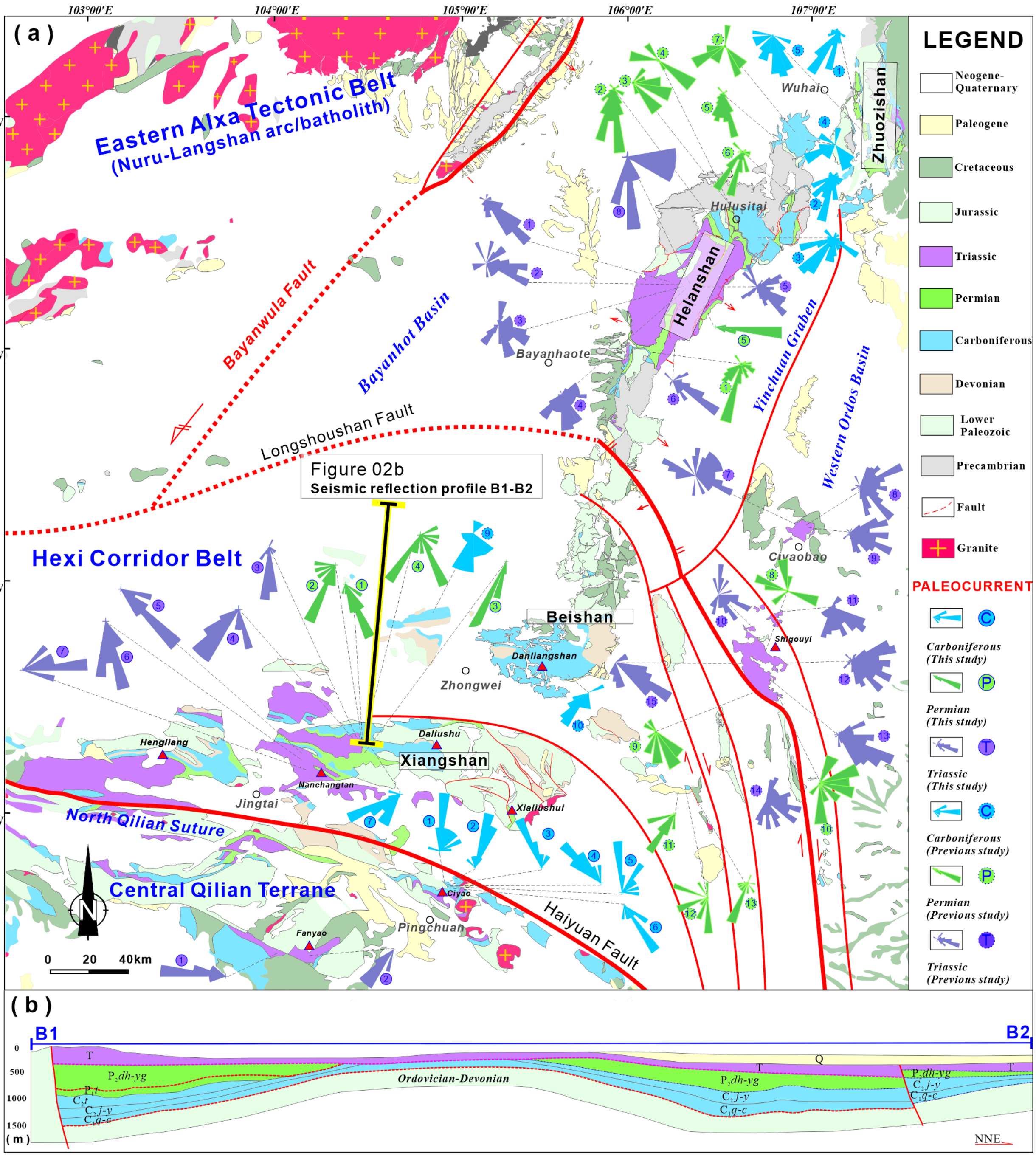

Figure 2. Geological maps of the Hexi Corridor. (a) Geological map showing the tectonic units of the study area (modified from Yang et al., 2025a). (b) Simplified and interpreted seismic reflection profile across the Eastern Hexi Corridor Belt, showing stratigraphic main units and their relations (modified from Shen et al., 2017). The insert rose diagrams illustrate paleocurrent directions obtained from Carboniferous, Permian and Triassic outcrops (published data sources are from Zhang, 2004; Li et al., 2009; Sun and Dong 2019; Zhao et al., 2021; Liu et al., 2022; Kou et al.,2022; Zhang et al., 2024; Yang et al., 2025a; Ma et al., 2025).

https://doi.org/10.5194/egusphere-2026-4406
Preprint. Discussion started: 4 September 2026

2 Tectonic outline and geological background of the EHCB and surroundings

The study area extends across the western NCB and EHCB (Fig. 1b), south of the Solonker-Engger Us suture. Ophiolites within this suture preserve relics of a Paleozoic to Triassic ocean (Xiao et al., 2003, 2015; Eizenhöfer et al., 2014, 2015; Eizenhöfer and Zhao, 2018; Eizenhöfer, 2019; Song et al., 2018, 2021, 2025). To the south lies the northern North China continental arc, including the Inner Mongolia continental arc (IMCA) in the east and the Shalazhashan and Nuru-Langshan continental arcs (NLCA) in the west. Most models regard the Engger Us suture as the southernmost limb of the PAO. Under this interpretation, the Changanchulu Ocean formed by back-arc spreading during southward subduction of the main Engger Us Ocean (Feng et al., 2013; Zheng et al., 2014; Sun and Dong, 2019; Tian et al., 2020, 2024; Song et al., 2024b). Other authors have suggested that the Chaganchulu suture marks the western NCB boundary, based on contrasting Precambrian geology between the ca. 1.5 Ga Shalazhashan Arc basement and the mainly ca. 2.6-1.8 Ga NLCA basement (Zhang et al., 2011, 2015; Zheng et al., 2022; Sun et al., 2024). Despite these differences, all scenarios agree that the NLCA was an Andean-type arc batholith that experienced two magmatic flare-ups at ca. 480-400 and 310-230 Ma (Fig. 3a; Liu et al., 2016, 2017; Song et al., 2021, 2023; Wang et al., 2022a, 2023a; Tian et al., 2024). Locally, ca. 1.4-0.8 Ga volcanic rocks and ca. 0.9 Ga felsic plutons occur along its western margin (Tian et al., 2019; Sun et al., 2024). Paleozoic to Triassic sedimentary units in the NLCA have been intensely eroded, except for a few outcrops adjacent to the Chaganchulu suture and in the Langshan area (Chen et al., 2016; Song et al., 2018, 2021). The NLCA can be traced eastwards to the IMCA, a ca. 500-230 Ma continental arc built on Archean-Paleoproterozoic NCB basement, with Mesoproterozoic-Neoproterozoic remnants preserved in the Bainaimiao terrane (Zhang et al., 2014; Eizenhofer and Zhao, 2018; Eizenhofer, 2019).

Inboard the arc belt is the Bayanhaote Basin, Helanshan, and western Ordos Basin, which display a nearly consistent Paleozoic-Triassic sequence comprising Cambrian to Ordovician carbonate-rich strata and Carboniferous-Triassic siliciclastic-dominated facies, bounded by a ~1.4 Ga depositional hiatus (Figs. 3b, c, d).

To the southwest, the western NCB is delimitated by the Longshoushan Fault from the North Qilian Orogen, which recorded the mid-Paleozoic shrinking and closure of the northern Proto-Tethys branches (Song et al., 2013; Dong et al., 2022; Sun and Dong, 2018, 2024). Generally, the North Qilian orogen consists of the Hexi Corridor and the North Qilian Suture zones, having been explained to as Cambrian to Ordovician subduction-accretionary complexes, affected by pervasive Paleozoic plutonism and metamorphism (Xu et al., 2010; Song et al., 2013; Dong et al., 2021; Fu et al., 2018a, 2020). The Central Qilian Terrene and its eastward extension in the North Qinling were both arcs created upon ca. 1100–900 Ma basement by ca. 520–450 Ma subduction of the North and South Qilian Ocean plates (Fu et al., 2018b; 2024). As thus, Cambrian to Ordovician geology of the EHCB was characterized by thick deep-water turbidites (Fig. 3b), significantly different from coeval shallow-water accumulation in the western NCB. Soon afterwards, alluvial-fluvial facies filled the EHCB foredeep from Silurian to Devonian, fed mostly by the Central Qilian Terrene (Yang et al., 2009, 2012; Xu et al., 2013; Sun and Dong, 2024).

This work focuses on Carboniferous-Triassic strata in the EHCB and the western Ordos (Fig. 2a). Sequences in both regions are relatively comparable, besides a few differences (Fig. 3). Commerce of Carboniferous sedimentation in the EHCB was

https://doi.org/10.5194/egusphere-2026-4406
Preprint. Discussion started: 4 September 2026

earlier than the western NCB, as Early Carboniferous sediments are absent in the NCB, indicating transgression onset from the west (Sun and Dong, 2020). Furthermore, much of Permian to Triassic succussions are absent in the Bayanhaote and northern EHCB, being recently demonstrated to be eroded at the end of Triassic (Yang et al., 2025a).

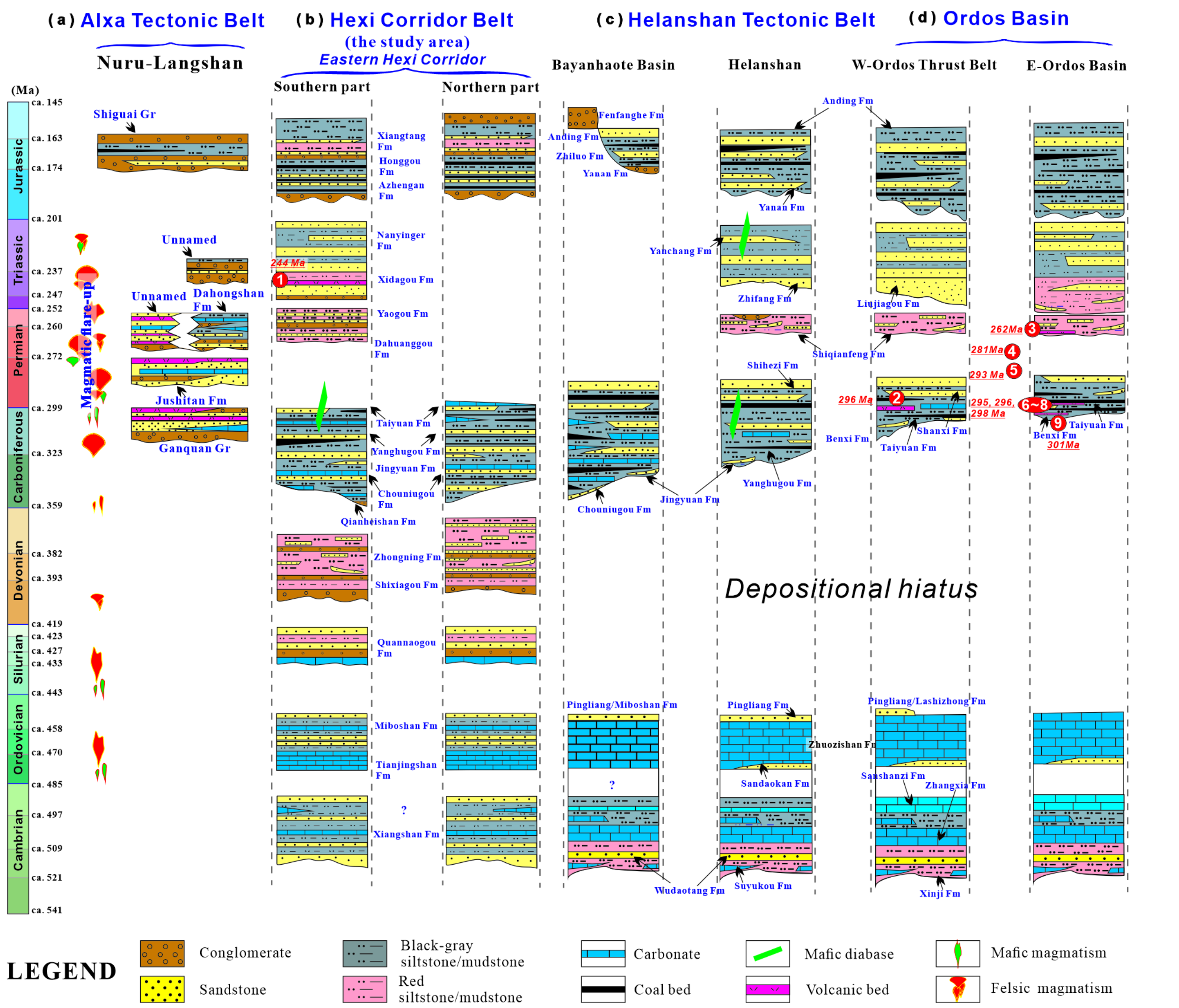

Figure 3. Schematic stratigraphic columns of Cambrian to Jurassic sedimentary successions of the Eastern Hexi Corridor Belt and surroundings (modified from Sun et al., 2024). Numerical ages and period divisions follow updated geologic time scale calibration defined in (Cohen et al. 2013). Abbreviation: Fm—Formation; Gr—Group. Tuff ages are from Yang et al. (2020) and Wu et al. (2021).

https://doi.org/10.5194/egusphere-2026-4406
Preprint. Discussion started: 4 September 2026

3 Stratigraphy and Sedimentology of Carboniferous–Triassic strata in the EHCB

Stratigraphy used here follows a recently updated proposal of lithostratigraphic subdivision and correlation of the Carboniferous, Permian, and Triassic in China, on basis of a review of biogeography, chronostratigraphy, cyclostratigraphy, and isotope stratigraphy (Shen et al., 2021, 2022; Tong et al., 2021; Li et al., 2021).

3.1 Carboniferous

Fang et al. (2014) yielded a detailed conodont succession study for the EHCB, and assigned Visean, Serpukhovian, Bashkirian to late Moscovian, Kasimovian to Asselian ages for the Chouniugou, Jingyuan, Yanghugou, and Taiyuan Fms, respectively. Hence, the Qianheishan Fm was deposited in Tournaisian (Tong, 1993; Tong and Li, 1994), and the upper Taiyuan Fm should be of early Permian age.

The Carboniferous sequence consists of grey-black colored mudstone and shale, with interbeds of quartz sandstone, coal, and limestone (Fig. 4). It was deposited in shallow marine setting, in view of hypermature siliciclastic deposition (Fig. 5a), carbonate deposition dominated by benthic fossils (Fig. 5b), mud crack and ripple (Fig. 5c), swaley (Fig. 5d) and planar (Fig. 5e) cross-bedding, coal-bearing shale (Fig. 5f), cross-bedded sandstone with ripple (Figs. 5g, h). Herringbone cross-bedding, mud flaser and lenticular bedding, as well as stromatolite, ammonite and gastropod, are common in all units, referring to high-energy, tide- and wave- dominated, delta-shoreface environments (Tong, 1993, 1994). At the early stage, the Carboniferous deposition was restricted locally with a maximum thickness of ~2000 meters around Zhongwei, thinning towards the south and north before dying out in the Qilian to the south and northwestern NCB to the north (Tong and Li, 1994; Yan, 2008). From the Chouniugou Fm deposition, the shallow-water system continued to onlap towards the NCB in its western margin (Fig. 3) and then covered the whole Ordos basin during the upper Yanghougou Fm deposition (i.e., the Benxi Fm).

https://doi.org/10.5194/egusphere-2026-4406
Preprint. Discussion started: 4 September 2026

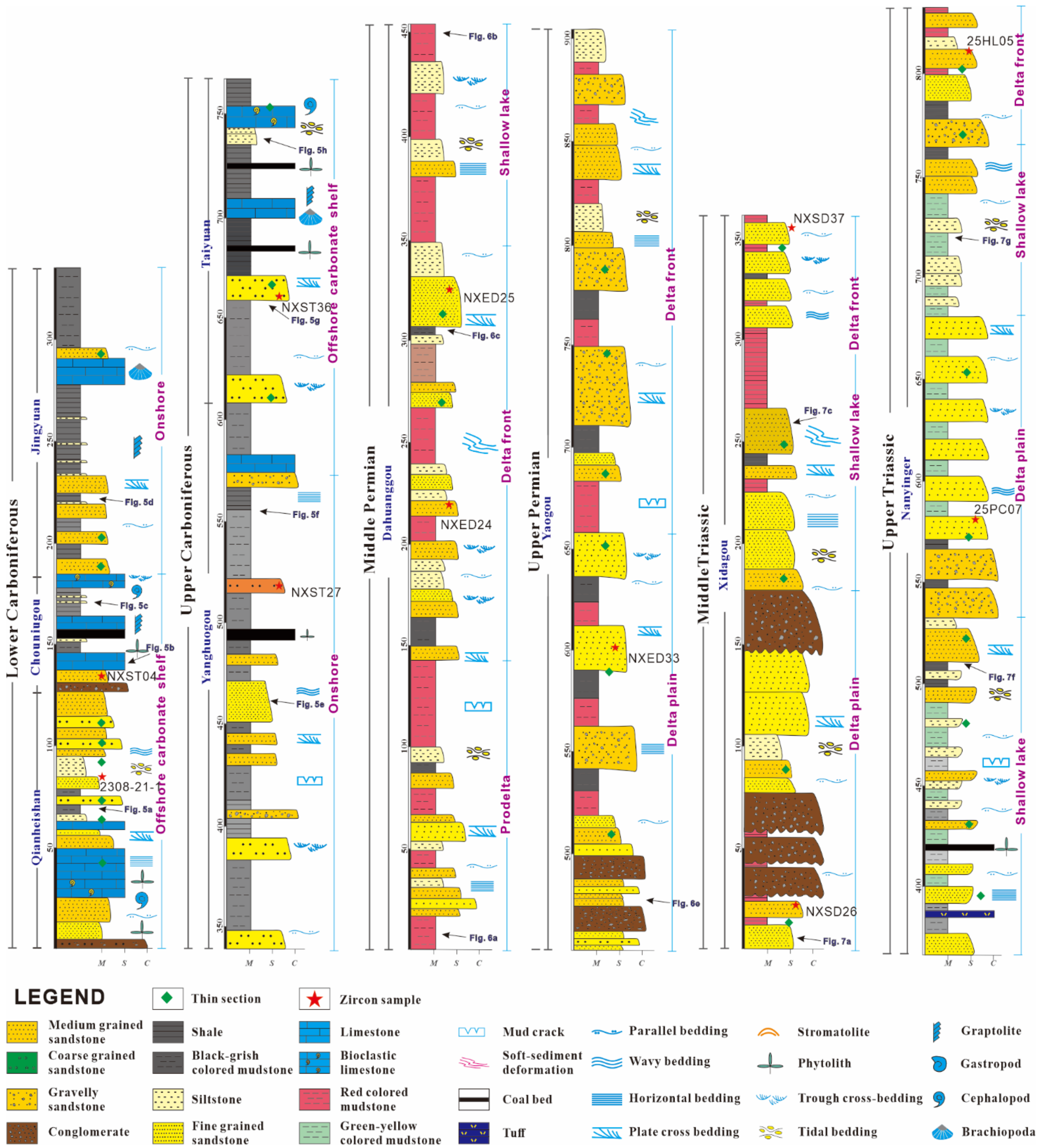

Figure 4. Stratigraphic columns showing lithological assemblages and interpreted sedimentary facies for the Carboniferous-Triassic strata in the Eastern Hexi Corridor. Red stars with red words showing approximate stratigraphic locations for detrital zircon samples of this study.

https://doi.org/10.5194/egusphere-2026-4406
Preprint. Discussion started: 4 September 2026

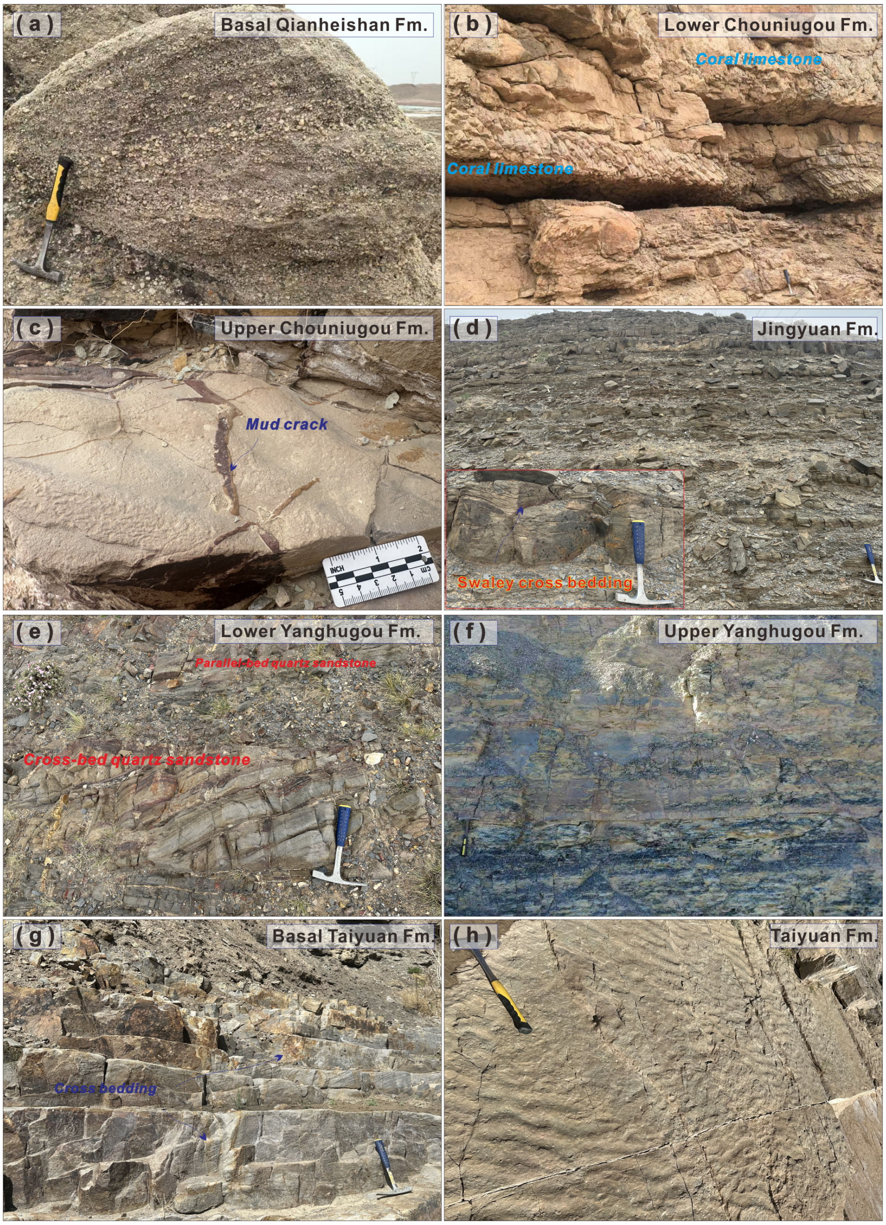

Figure 5. Representative photographs of the Carboniferous strata in the study area, illustrating stratigraphic, petrological, and sedimentological characteristics. Scales used include geological harmer (25 cm long) and card (5 cm long). (a) Cross-bedded fine-grained quartz conglomerate at the base of Qianheishan Fm, Xialiushui Section. (b) Two coral limestone interbeds within the Chouniugou Fm, Xialiushui Section. (c) Ripple marks and mud cracks of sandstones in the upper Chouniugou Fm, Daliushu Section. (d) Alternation of sandstone and silty mudstone of the Jingyuan Fm, with insert showing storm-generated swaley cross bedding, Danliangshan Section. (e) Cross- and parallel-bedded quartz sandstones of the Lower Yanghugou Fm, Nanchangtan Section. (f) Sandstone interbedded within black shale of the upper Yanghugou Fm, Nanchangtan Section. (g) Medium-bedded plate cross-bedded sandstone of the basal Taiyuan Fm, Nanchangtan Section. (h) Ripple marks on top of sandstones of the Taiyuan Fm, Ciyao Section.

https://doi.org/10.5194/egusphere-2026-4406
Preprint. Discussion started: 4 September 2026

3.2 Permian

Previous proposal argued that Carboniferous-Permian deposition was continuous (Xu et al., 1993) and assigned a Cisuralian age for the Dahuangou Fm and Lopingian age for the Yaogou Fm, respectively (Shen et al., 2021). Luo and Wang (1992) assumed a Carboniferous-Permian paraconformity between the Taiyuan and Dahuanggou Fms.

A sandstone sample from the basal Dahuanggou Fm yields 46 ages younger than 290 Ma, the youngest 8 ages generate a weighted mean age of 268 ± 3 Ma (Fig. 6a), solidly constraining its deposition age to be no older than mid-Permian. The Yaogou Fm samples (Figs. 6b-d) also contain a number of zircons younger than ca. 260 Ma, limiting deposition age of the Yaogou Fm to be Late Permian. Therefore, we suggest a paraconformity spanning at least ~30 Ma in Early–Middle Permian. The unconformity can directly be viewed from interpreted seismic reflection profile, as the Taiyuan Fm is absent in the north (Fig. 2b), where Permian-Triassic strata are all absent (Fig. 3b).

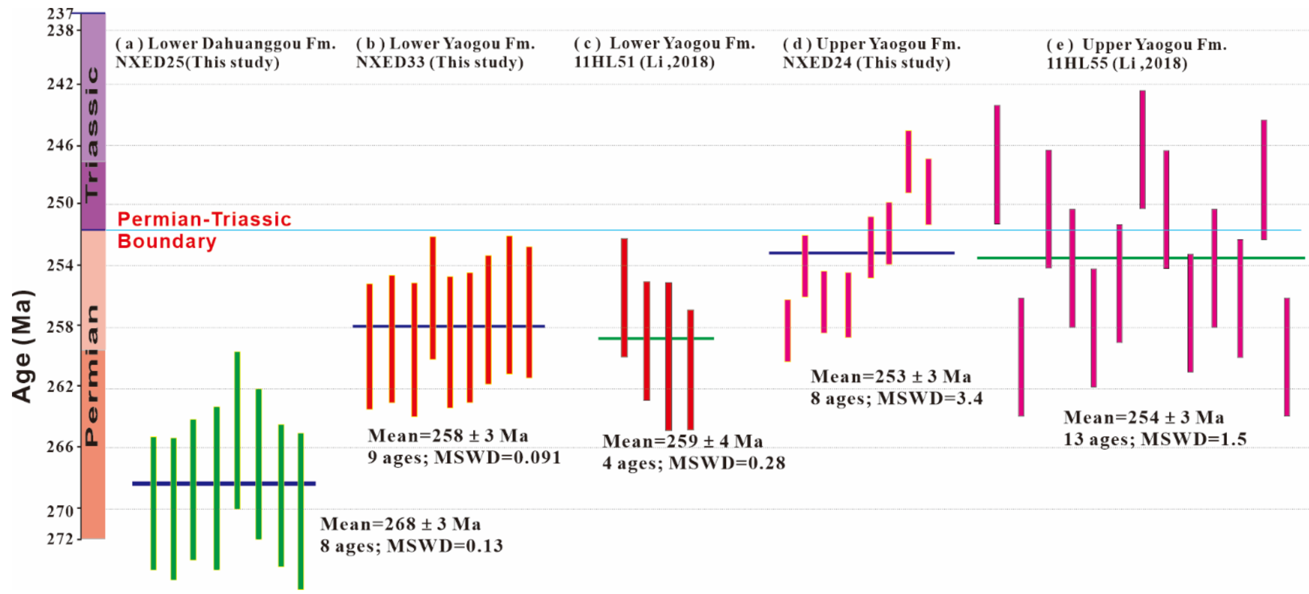

Fig. 6. Youngest detrital zircon ages for the Permian Dahuanggou and Yaogou Fms from this study and (Li, 2018).

The Dahuanggou Fm rests uncomfortably on the Taiyuan Fm (Fig. 7a), and in turn uncomfortably covered by the Yaogou Fm (Fig. 7b). The Dahuanggou and Yaogou Fms are of non-marine origin, inferred from that mudstone layers are generally red colored (Fig. 4, 7). Thick- to massive- beds of red mudstone, which generally contain calcareous clay interbeds or concretions (Fig. 7b), were interpreted to be formed in seasonal lake environments (Shen et al., 2021). The interbedded greyish-green-color, coarse-grain, cross-bed sandstones (Fig. 7c) represent delta depositions (Wei et al., 2011). The Yaogou Fm consists of increasing amounts of gravelly sandstone layers (Fig. 7d) deposited in fluvial to alluvial fan settings (Kou et al., 2022). A ~2-m thick conglomerate layer occurs at its base (Fig. 7e), containing a complexity of gravels of diverse lithologies, such as, chert, quartz, and granite (Fig. 7f).

https://doi.org/10.5194/egusphere-2026-4406
Preprint. Discussion started: 4 September 2026

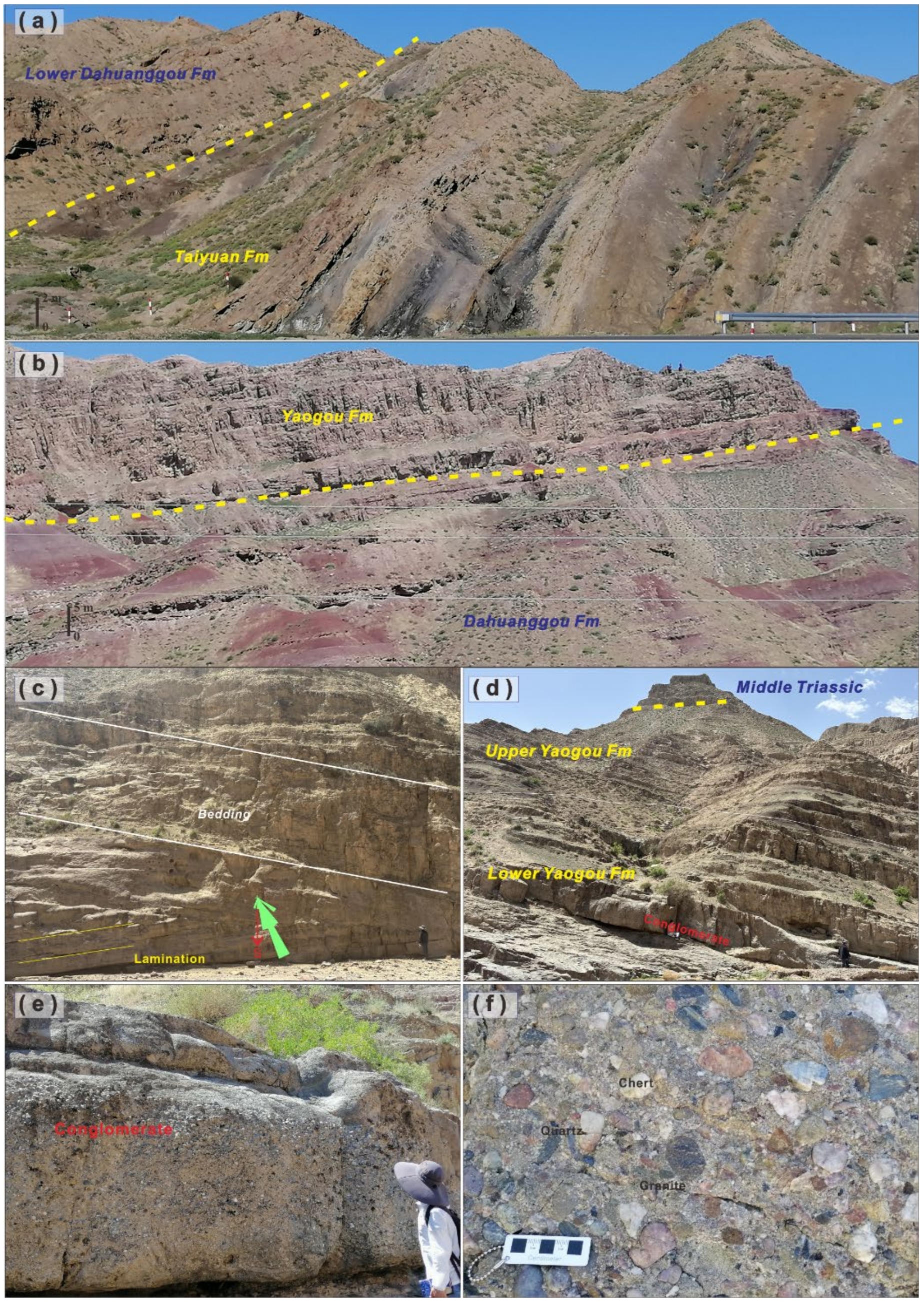

Figure 7. Representative photographs of the Permian strata in the study area, illustrating stratigraphic, petrological, and sedimentological characteristics.Scales used include geologist (175 cm long) and card (5 cm long). (a) The Carboniferous-Permian paraconformity boundary at the Nanchangtan Section. (b) Paraconformity between the Dahuanggou Fm and Yaogou Fm at the Nanchangtan Section. (c) Large-scale plate cross bedding of thick-bedded gravelly sandstone at the bottom of the Yaogou Fm, with insert showing paleocurrent directions, Nanchangtan Section. (d) Distant view of the Permian-Triassic boundary and conglomerate within the lower Yaogou Fm, Nanchangtan Section. (e) A ~1.5 m thick conglomerate bed of the lower Yaogou Fm, Nanchangtan Section. (f) Conglomerate contains pebbles of varying lithologies, Nanchangtan Section.

https://doi.org/10.5194/egusphere-2026-4406
Preprint. Discussion started: 4 September 2026

3.3 Triassic

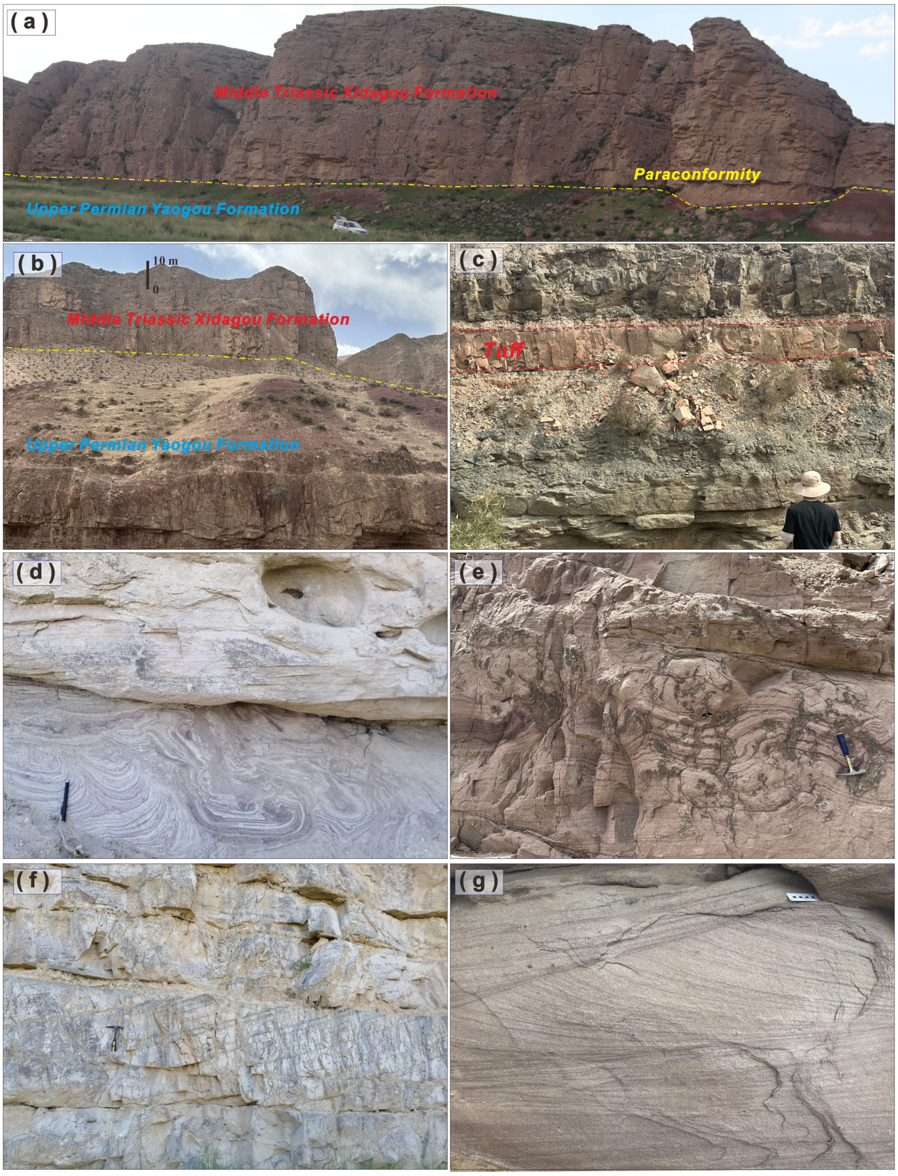

Figure 8. Representative photographs of the Triassic strata in the study area, illustrating stratigraphic, petrological, and sedimentological characteristics. Scales used include car (5 m long), pen (10 cm long), geological harmer (25 cm long), and geologist (175 cm long). (a) Paraconformity between the Upper Permian Yaogou Fm and the Middle Triassic Xidagou Fm at the Hengliang Section. (b) Paraconformity between the Upper Permian Yaogou Fm and the Middle Triassic Xidagou Fm at the Nanchangtan Section. (c) Soft sediment deformation of the Xidagou Fm at the Nanchangtan Section. (d) Soft sediment deformation of the Xidagou Fm at the Nanchangtan Section. (e) Plate cross beddings of quartz sandstone of the Xidagou Fm at the Nanchangtan Section. (f) Quartz sandstone contains trough cross-beddings of the lower Nanyinger Fm at the Jingtai Section. (g) Tuff interlayers within the greyish mudstone of the Nanyinger at the Ciyao Section.

The Early Triassic successions are absent in the EHCB, and contact between the Triassic Xidagou and underlying Permian Yaogou Fms is a paraconformity (Fig. 8a, b). The Early Triassic sequence is categorized into the Xidagou and Nanyinger Fms, which have been formerly considered to be deposited in Late Triassic. Tuffs from the upper Xidagou Fm (Fig. 8c) yielded two weighted mean ages of 241±2 Ma and 245±3 Ma (Xin et al., 2013a, b). The Xidagou Fm contains typical Middle Triassic plant fossils (Du, 1985; Sun and Xu, 1988). Thus, the Xidagou Fm should be Middle Triassic in age, corresponding to the Chang 10~7 Members in the adjacent Ordos (Tan et al., 2022). The Xidagou Fm is sandstone-rich, characterized by common presence of soft-sediment deformations (Fig. 8d, e), implying a delta setting (Li et al., 2009; Guo et al., 2019). The Upper Triassic Nanyinger Fm corresponds to Chang 6~1 Members in the Ordos Basin (Deng et al., 2018; Guo et al., 2019). It is composed of gray-green cross-bedded sandstone (Fig. 8f, g) at its base, and fines upwards to lacustrine shale and mudstone in the middle section, before grading into fluvial facies green-yellow colored mudstone and siltstone (Fig. 4).

4 Sampling, analytical methods, and results

Detailed sampling locations and analytical methods are provided in the **Appendices**.

4.1 Paleocurrent reconstruction

The Fig. 2 displays reconstructed directions from the EHCB and western NCB. The Carboniferous data are mainly grouped in two directions. In the southern EHCB, the paleocurrent directions are mainly northward, instead, data from the northern EHCB direct to the south. Paleocurrent indicators of the Permian alluvial fan and fluvial facies show a unimodal pattern towards the south, indicating that that detrital materials of the EHCB and western NCB were primarily routed from the north. As the same as Permian, the unimodal southeastward-directed flow pattern indicates that the Triassic sediments in the EHCB were transported by south-flowing paleodranage systems, whereas data from the western Ordos are southeast-oriented, suggesting that the Triassic detrital materials were mainly derived from the northwest.

4.2 Petrography and framework composition of sandstones

Samples from the Carboniferous-Triassic successions in the EHCB are textural immaturity and submaturity. Framework grains are poorly- to moderately- sorted and generally have irregular polygonal shapes with low roundness and sphericity (Supplementary Fig. 1).

The Carboniferous sandstones are mainly quartz (average 84%), monocrystalline quartz is common, followed by lithic fragments (average 10%), with rare amounts of feldspars; the lithic fraction consists mainly of sedimentary rock fragments. The Permian ones are generally feldspathic arenite to sub-litharenite, composed mainly of subangular- to angular shaped quartz

https://doi.org/10.5194/egusphere-2026-4406
Preprint. Discussion started: 4 September 2026

grains (48%–85%; average 63%). Plagioclase feldspar (average 10%) and K-feldspar (average 11%) are equal. Lithic fragments are mostly volcanic. The Triassic sandstones contain increasing amounts of Quartz grains and metamorphic lithic fragments, accounting for 76% and 10% on average.

On the Qt-F-L diagram, most samples plot within the recycled orogen provenance field (Fig. 9a). Carboniferous and Triassic samples largely fall in the recycled orogen field, whereas most Permian samples cluster near the boundary between the recycled orogen, continental block, and magmatic arc provenance fields. (Fig. 9b). On the Qp-Lv-Ls diagram, most modal data plot in the mixed orogenic source field, although their distribution is relatively scattered (Fig. 9c).

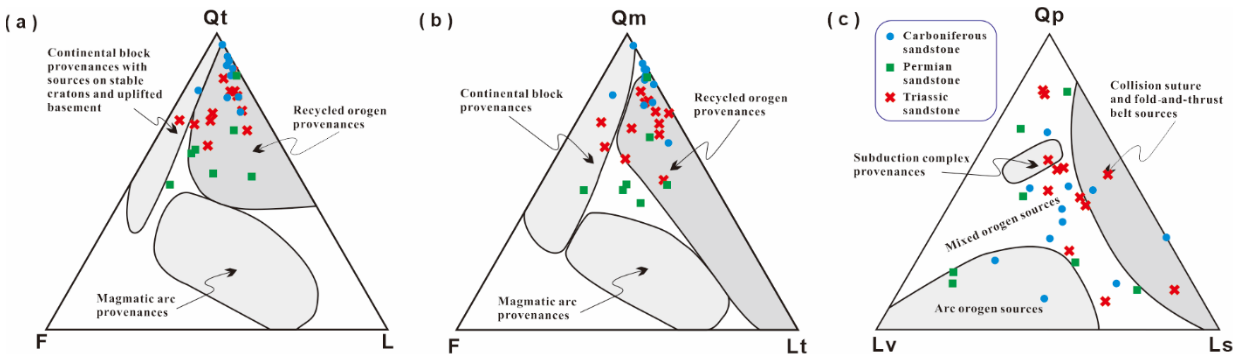

Figure 9. Standard ternary diagrams for Carboniferous, Permian and Triassic sandstone modal composition data from the Eastern Hexi Corridor Belt and surroundings. (a-c) Provenance fields (after Dickinson and Suczek, 1979; Dickinson, 1988). Qt—total quartz; Qm—monocrystalline quartz; Qp—polycrystalline quartz; K—K-feldspar; Pl—plagioclase; L—lithic fragment; Lm—metamorphic lithic fragments; Ls—sedimentary lithic fragments; Lv—volcanic lithic fragments; Qt = Qm + Qp; F =K + Pl; Lt = L + Qp.

4.3 Zircon U-Pb geochronology

The Qianheishan Fm sample 2308-21-1 yielded 97 concordant analyses from 100 zircon grains. The dated grains span 3443-394 Ma (Fig. 10a, b), with the principal population centered at 432 Ma (55 ages). Minor populations occur at 975 Ma and 2436 Ma.

For sample NXST04 from the Chouniugou Fm, 92 of 100 analyses were retained as reliable ages. The ages range from 3570 to 374 Ma (Fig. 10c, d). The spectrum is dominated by a 441 Ma peak (56 ages), accompanied by smaller peaks at 998 Ma, 2024 Ma, and 2510 Ma.

Sample NXST27 from the Yanghugou Fm produced 90 concordant ages from 100 analyzed grains. The age range is 2650-309 Ma (Fig. 10e, f). Two dominant populations are present, with peaks at 435 Ma (27 ages) and 2512 Ma (16 ages).

In sample NXST36 from the Taiyuan Fm, 95 concordant ages were obtained from 100 analyzed grains. These ages extend from 2790 to 379 Ma (Fig. 10g, h). The main peak is at 418 Ma (27 ages), whereas subordinate populations peak at 927 Ma and 2024 Ma.

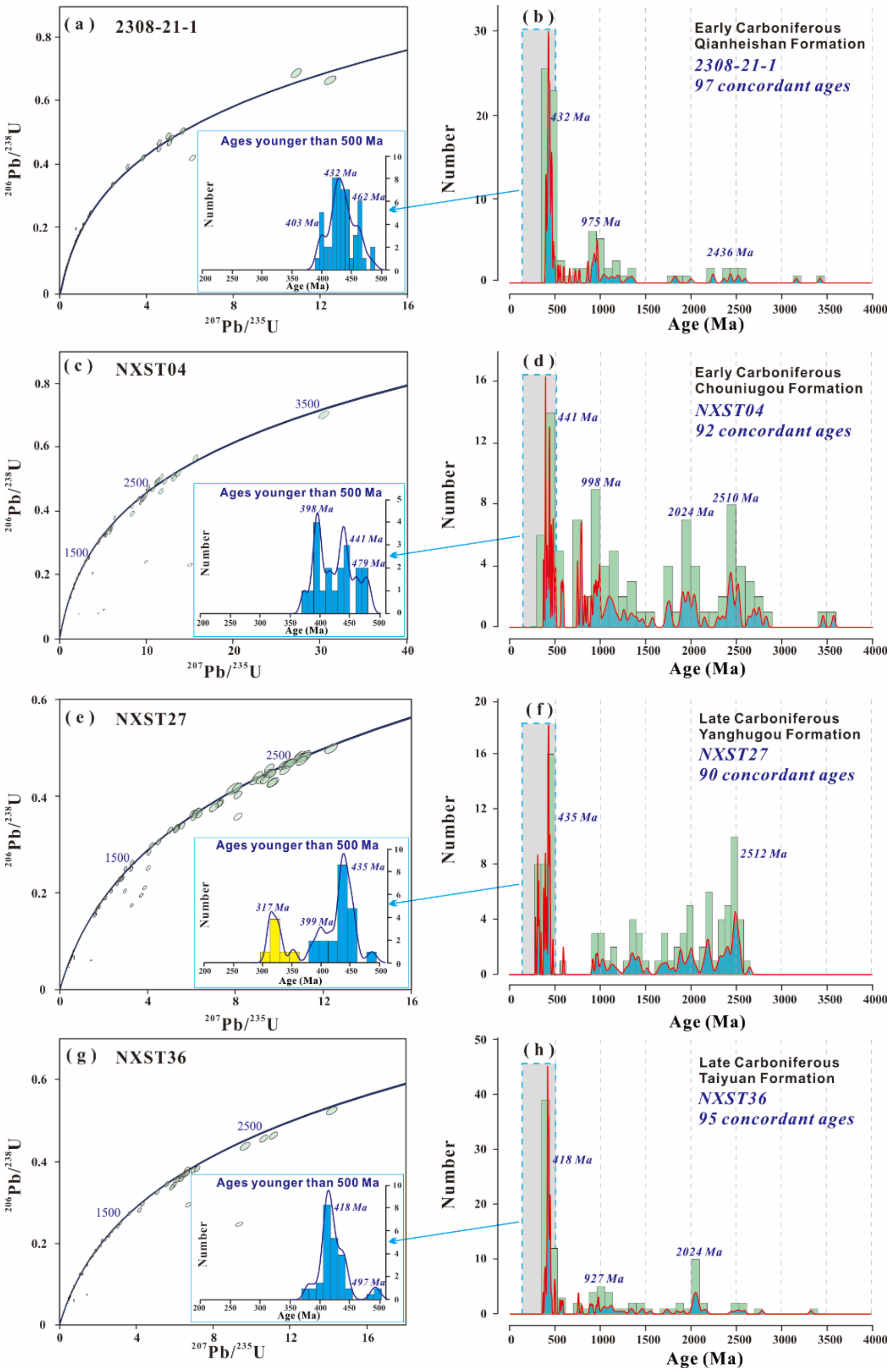

245 **Figure 10. (a, c, e, g) Concordia plots and (b, d, f, h) frequency histograms with relative probability density curves for detrital zircon U-Pb ages from Carboniferous sandstone samples. Only analyses younger than 500 Ma are included in the concordia panels. Ellipses denote individual analyses and show 2 sigma uncertainties.**

https://doi.org/10.5194/egusphere-2026-4406
Preprint. Discussion started: 4 September 2026

The Dahuanggou Fm sample NXED25 provided 97 reliable ages from 100 analyses. Ages range from 2499 to 256 Ma (Fig. 11a, b). Apart from two older grains at 2500 Ma and 1700 Ma, 80 ages in the range 501–256 Ma constitute a unimodal age peak at 277 Ma.

Sample NXED24 from the Yaogou Fm yielded 94 concordant ages from 100 analyzed grains. The age range is 2555-245 Ma (Fig. 11c, d). The distribution contains two major peaks, at 266 Ma (40 ages) and 415 Ma (39 ages).A second Yaogou Fm Sample, NXED33, produced 99 reliable ages between 1607 and 251 Ma (Fig. 11e, f). Three scattered older ages occur at 1520 Ma, 950 Ma, and 730 Ma. Most analyses, 75 grains between 328 and 251 Ma, form a single peak at 268 Ma.

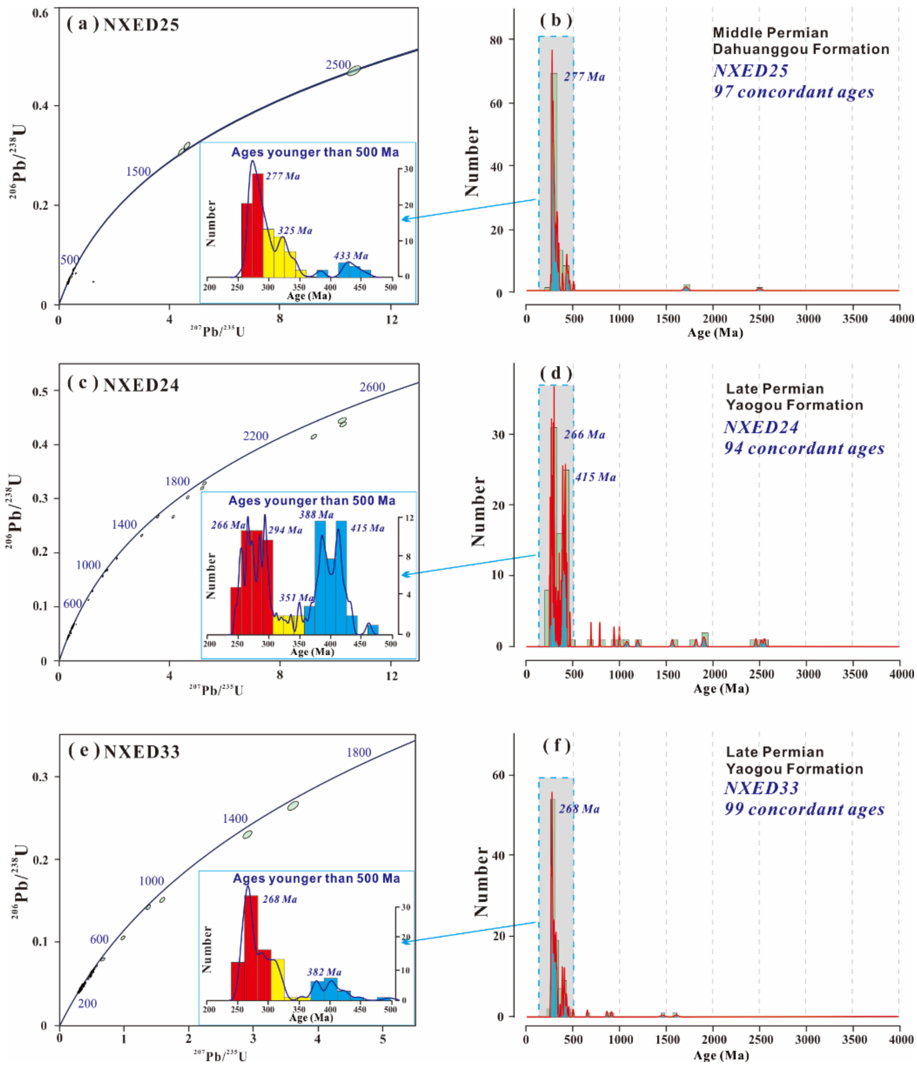

Figure 11. (a, c, e) Concordia plots and (b, d, f) frequency histograms with relative probability density curves for detrital zircon U-Pb ages from Permian sandstone samples. Only analyses younger than 500 Ma are included in the concordia panels. Ellipses denote individual analyses and show 2 sigma uncertainties.

https://doi.org/10.5194/egusphere-2026-4406
Preprint. Discussion started: 4 September 2026

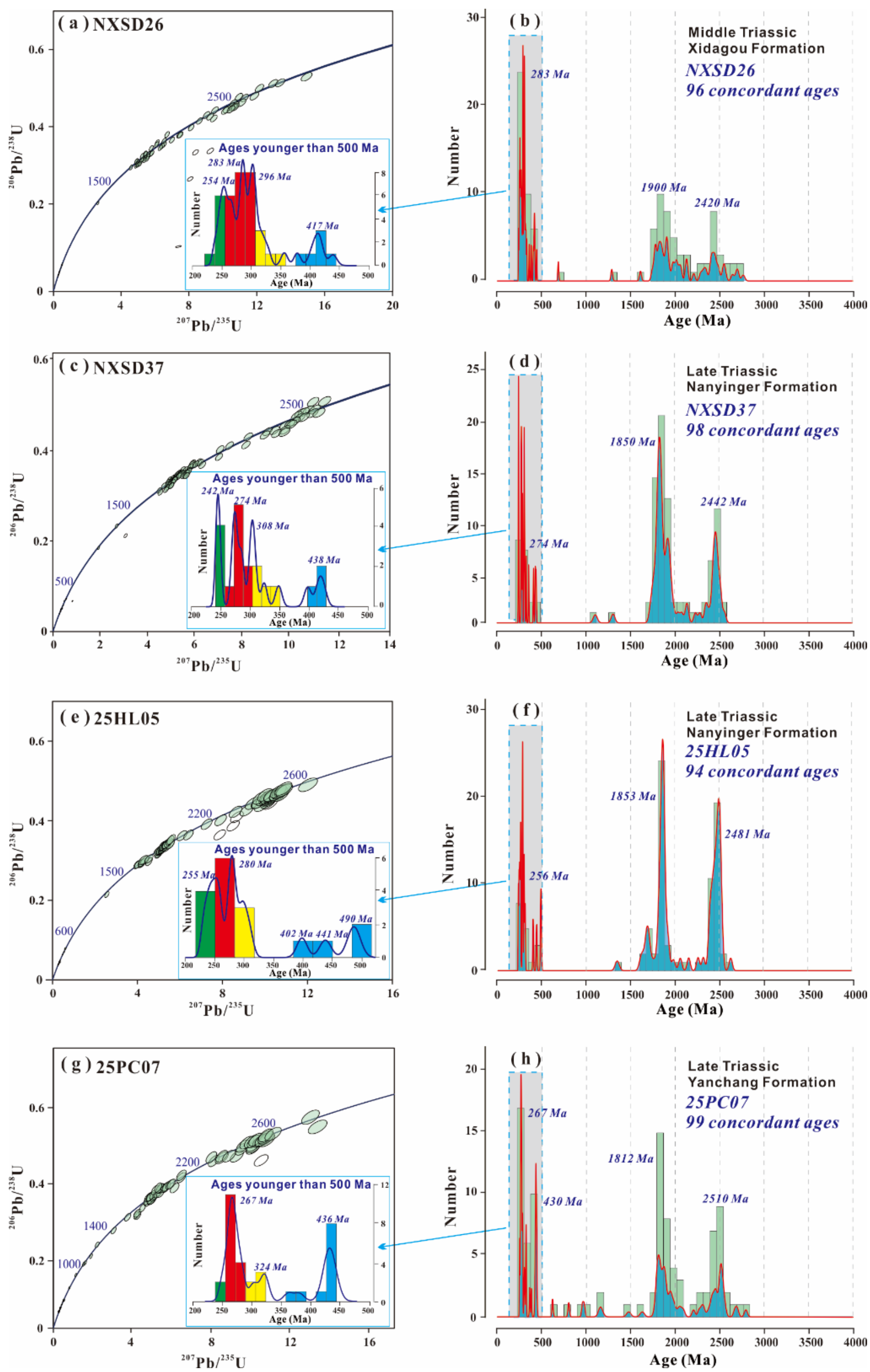

Figure 12. (a, c, e, g) Concordia plots and (b, d, f, h) frequency histograms with relative probability density curves for detrital zircon U-Pb ages from Triassic sandstone samples. Only analyses younger than 500 Ma are included in the concordia panels. Ellipses denote individual analyses and show 2 sigma uncertainties.

https://doi.org/10.5194/egusphere-2026-4406
Preprint. Discussion started: 4 September 2026

Sample NXSD26 was obtained from Xidagou Fm. One hundred zircon spots were analyzed in the core region of 100 grains, which generated 96 concordant ages of 2844–237 Ma (Fig. 12a, b). The age distribution is characterized by dominant age peaks at 283 Ma (39 ages), 1900 Ma (36 ages), and 2420 Ma (16 ages).

Sample NXSD37 of Nanyinger Fm generated 99 reliable results, spanning 2561-240 Ma (Fig. 12c, d). The ages are clustered in three main age groups of 2081–1726 Ma (50 ages), 2561–2138 Ma (26 ages), and 440–240 Ma (19 ages), These groups define peaks at 1850 Ma, 2442 Ma, and 274 Ma.

The Yanchang Fm sample 25HL05 from the Helanshan area retained 94 reliable ages from 100 analyses. The ages range from 2634 to 231 Ma (Fig. 12e, f). Two large populations peak at 1853 Ma (37 ages) and 2481 Ma (35 ages), and a smaller population peaks at 256 Ma (13 ages).

Sample 25PC07 from the Nanyinger Fm in the Pingchuan area yielded 99 reliable analyses out of 100. Ages span 2801-249 Ma (Fig. 12g, h). The spectrum contains peaks at 267 Ma (16 ages), 430 Ma (10 ages), 1812 Ma (26 ages), and 2510 Ma (18 ages). A relative age gap separates the 1600-600 Ma interval.

4.4 Hf isotope data in zircon

In-situ Lu–Hf isotopic analyses were performed on 75 detrital zircon grains with U–Pb ages ranging from 450 to 250 Ma. The resulting isotopic compositions are reported in Supplementary Table 6. Hf isotopic composition of zircon (n=75) shows $^{176}Lu/^{177}Hf$ ratios between 0.000369 and 0.00307 with initial $^{176}Hf/^{177}Hf$ values for (0.282012–0.282899). The εHf(t) values mainly range from -19.978 to 11.586, corresponding to ages (T_{DM2}) of 2.59–0.66 Ga. As illustrated in Fig. 13, the εHf(t) values display a peak between 320 and 290 Ma, and two troughs at ca. 380–330 Ma and 285–260 Ma.

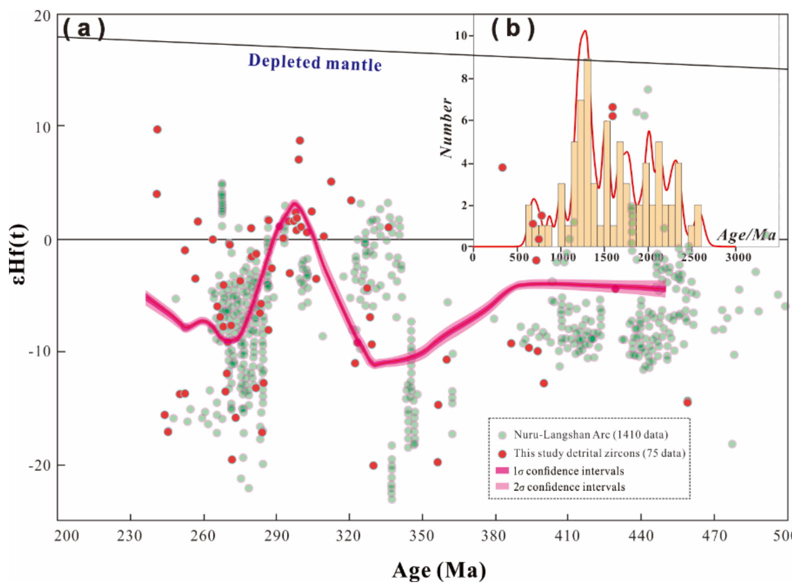

Figure 13. (a) εHf(t) v. $^{207}Pb/^{206}Pb$ ages (Ma) diagram for detrital zircons with ages of ca. 500–200 Ma from Carboniferous, Permian and Triassic sandstones from the Hexi Corridor, data for the Nuru-Langshan Continental Arc are from Song et al., (2024). (b) The inserted histogram shows T_{DM2} ages of detrital zircons.

https://doi.org/10.5194/egusphere-2026-4406
Preprint. Discussion started: 4 September 2026

5 Discussions

5.1 Multi-stage provenance shifts in forearc and retroarc basins of the NLCA

5.1.1 A review of new data and known geologic observations

Paleocurrent data from Carboniferous strata in the southern EHCB indicate sediment influx from the south, whereas the northern EHCB and western NCB were supplied by a northern provenance (Fig. 2a). Detritus from these opposing source areas mingled around the Zhongwei depocenter (Tong, 1994). A southerly source for the southern during Carboniferous is compatible with the fact that there are no coeval strata in the Qilian Orogen to the south of Pingchuan (Tong and Li, 1994). Most Permian and Triassic sections record consistently south-directed paleocurrents, whereas Triassic strata in western Ordos record a southeast-flowing drainage system.

Framework-grain analyses indicate that Carboniferous, Permian, and Triassic sediments were mainly supplied by mixed recycled-orogen and continental-block provenances (Fig. 9a). Compositional maturity decreases upward because Permian-Triassic samples contain more feldspar and lithic grains (Fig. 9b). Polycrystalline quartz and sedimentary lithic fragments are abundant in Carboniferous and Triassic samples, whereas Permian samples are dominated by volcanic lithic fragments and contain few sedimentary fragments (Fig. 9c).

The compiled Carboniferous, Permian, and Triassic sandstone detrital-zircon U-Pb age patterns are distinct (Fig. 14). Carboniferous samples yield ages of 3570-309 Ma (Fig. 14a, b). Carboniferous ages are rare, accounting for only 1.87%, whereas older ages dominate and define four major peaks at ca. 434 Ma, 974 Ma, 2068 Ma, and 2528 Ma. Permian age spectra range from 2555 to 250 Ma (Fig. 14c, d), with two major age clusters at 375-250 Ma (206 ages; approximately 70%) and 500-377 Ma (63 ages; 22%), defining peaks at 272 Ma and 417 Ma, respectively. Triassic samples are concentrated at ca. 500-220 Ma and ca. 2700-1700 Ma, with a relative age gap between ca. 1600 and 500 Ma (Fig. 14e, f). Four sub-clusters display age peaks at 269 Ma, 438 Ma, 1865 Ma, and 2502 Ma.

https://doi.org/10.5194/egusphere-2026-4406
Preprint. Discussion started: 4 September 2026

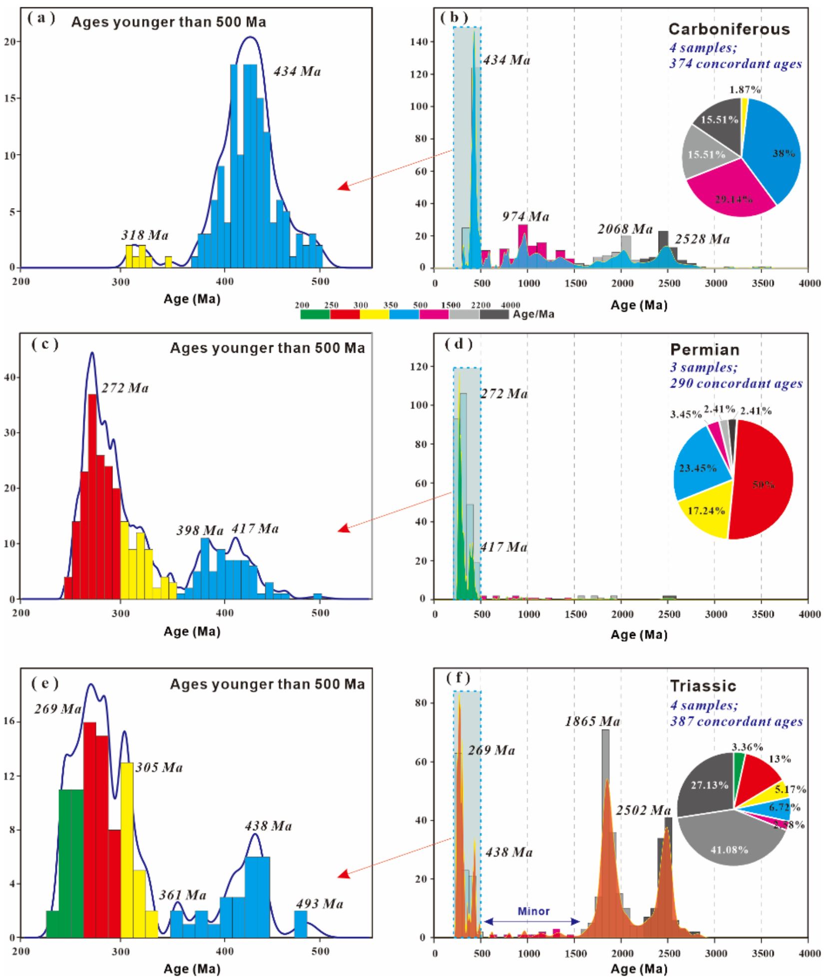

Figure 14. Frequency(bars) and probability density distribution (curves) of ages for potential provenances; (a) Eastern Hexi Corridor retro arc; (b) Nuru-Langshan Forearc; (c) Western Ordos; (d) Eastern Ordos. See references for all samples in Supplementary Table 1.

5.1.2 Evolving provenance from Carboniferous to Triassic

We synthesized 91 detrital zircon U-Pb age results reported in the NLCA forearc, as well as the retroarc EHCB, eastern Ordos, and western Ordos (Fig. 15). Potential sources for the study area include the northern North China Continental Arc to the north and the Qilian-Qinling Orogen to the south. We found that it can easily distinguish the northerly and southerly provenances, as sources from both sides have rather distinct age patterns. A minor number of ages or even an age gap occurs in the range of ca. 1.7–0.6 Ga for the northern NCB and the arc belt built upon it, whereas Meso–Neoproterozoic basements are widespread in the Qilian-Qinling. Another diagnostic discrimination is that Late Paleozoic magmatism is almost absent in the Qilian-Qinling, however, plutons within the northern North China Continental Arc were pervasively emplaced then.

https://doi.org/10.5194/egusphere-2026-4406
Preprint. Discussion started: 4 September 2026

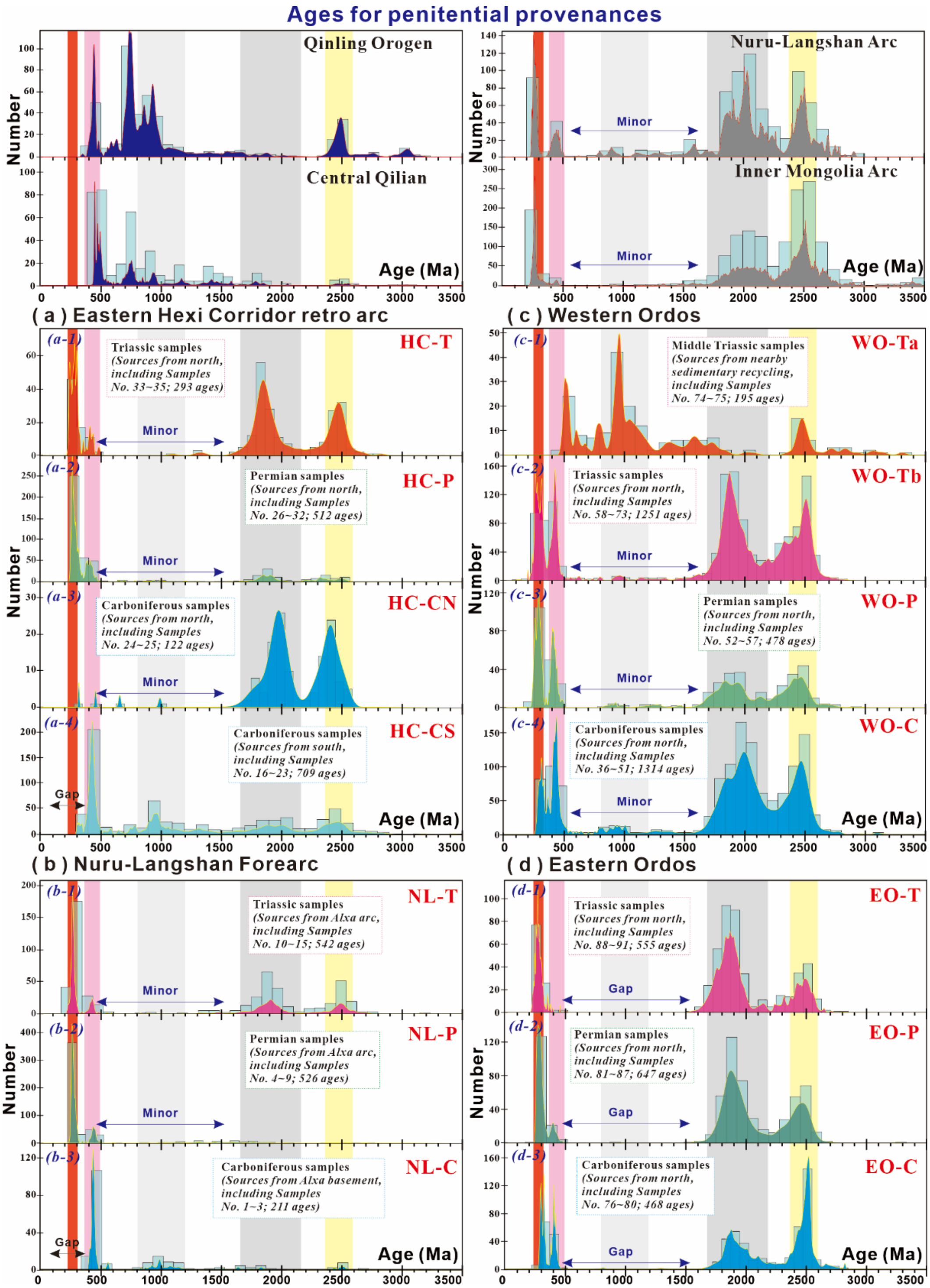

Figure 15. Frequency (bars) and relative probability density distribution (curves) of ages for sandstone samples from Carboniferous Permian and Triassic strata. including ages younger than 500 Ma resulting. The ellipse represents the percentage of age distribution.

https://doi.org/10.5194/egusphere-2026-4406
Preprint. Discussion started: 4 September 2026

5.1.2.1 Carboniferous Stage

Paleocurrent data and stratigraphic correlation (Tong and Li, 1994) imply a two-side sediment-supply mode in Carboniferous, with deposition center around Zhongwei. The Central Qilian and western NCB were both paleo-highlands then, given absence of coeval strata there. This view is further confirmed by two totally different age patterns for detritus in the southern and northern EHCB (Fig. 15a). The former has a typical Central Qilian basement pattern, dominated by ca. 1000–800 Ma and ca. 550–400 Ma age clusters that correspond to Neoproterozoic Rodinia-forming orogenesis (Wu et al., 2016; Fu et al., 2018b; Peng et al., 2019) and the mid-Paleozoic closure of the northern Proto-Tethys (Xiao et al., 2009; Song et al., 2013; Zuza et al., 2018; Zhang et al., 2023). Paucity of Carboniferous tectonic signatures makes it easily distinguishable from a northerly arc source but is coherent with a magmatic lull after Devonian throughout the Qilian Orogen (He et al., 2024). Strata in the northern EHCB display south-directed paleocurrent data and detrital zircon U-Pb ages clustering in the range of ca. 2700–1700 Ma with less than 2% ages younger. We interpret these samples of a mostly NCB basement source in the western Ordos Basin. Although sandstone discrimination results (Fig. 9) reveal a mixed craton and orogen source, this does not conflict with previous conclusions, as the NCB and Qilian basements are both ancient orogens (Zhao et al., 2012; Song et al., 2013). Enrichment of quartz grains may reflect long-term basement weathering in a stable setting.

In the NLCA forearc, Carboniferous sandstones have no signs of ca. 350–300 Ma ages but contain numerous ca. 500–400 Ma and ca. 1000–800 Ma ages (Fig. 15b), sources of which can be correlated to 2 distinct plutonism stages in Early Paleozoic and Neoproterozoic (Song et al., 2020, 2024b; Zheng and Zhang, 2024), respectively. For the northern Ordos (Fig. 15c, d), late Carboniferous sediments all have age profiles characterized by 2 distinct groups of Paleozoic and Neoarchean to Paleoproterozoic, separated by age gap between 1600 Ma and 550 Ma. The Late Paleozoic detrital zircons are not substantial in northern EHCB; however, the western and eastern Ordos samples, which are mostly end-Carboniferous in age, contain a considerable number of Paleozoic arc components. The highly consistent age relation and southward flowing deposition system (Li et al., 2019; Guo et al., 2019) attitude their sources to the IMCA, lasting to Triassic as there are no changes among age spectra (Eizenhöfer and Zhao, 2018; Sun and Dong, 2020).

5.1.2.2 Permian–Triassic Stage

The Permian age spectra of the EHCB retroarc and Nuru-Langshan forearc strata are both dominated by ~85 % number of Paleozoic-age zircons, different from those of coeval units in the Ordos where increasing amount of sediment contribution of the ca. 2700–1700 Ma IMCA basement materials were dispersed to the basin. These Paleozoic ages fall into 2 individual clusters with age peaks at ca. 430 Ma and 275 Ma, matching well with 2 subduction-induced magmatic flare-ups in the NLCA (Liu et al., 2016; Song et al., 2018, 2024; Tian et al., 2021, 2024; Zheng and Zhang, 2024). Although limited, Precambrian ages also constitute 2 groups, with age peaks corresponding to 2 major tectonic events that led to the formation and assembly of the western NCB (Zhao et al., 2012; Zhang and Gong, 2018). The Triassic samples have ~60 % of ca. 2700–1700 Ma

https://doi.org/10.5194/egusphere-2026-4406
Preprint. Discussion started: 4 September 2026

detritus that implies increasing sediment supply of the NLCA basement. The Meso- to Neoproterozoic geologic quiescence is also compatible with the paucity of ca. 1600–600 Ma ages.

The εHf values for 500–220 Ma aged detrital zircons show a strong overlapping with those for coeval magmatic rocks in the NLCA, with a same evolution trend with time (Fig. 13). The multi-dimensional scaling (MDS) plot in Fig. 16 depicts the dissimilarities among samples and potential source terranes. The Carboniferous Nuru-Langshan forearc (NL-C) and southern EHCB (HC-CS) falls in the range far away from the continental arc provenance region that involves most of Permian–Triassic samples. The northern EHCB (HC-CN) plot also occurs in the second source domain, because the NCB basement has Precambrian ages consistent with the basement of NLCA and IMCA. The third source region consists of the Permian NLCA (NL-P) and EHCB (HC-P) samples, because of the enrichment of Paleozoic arc contributions.

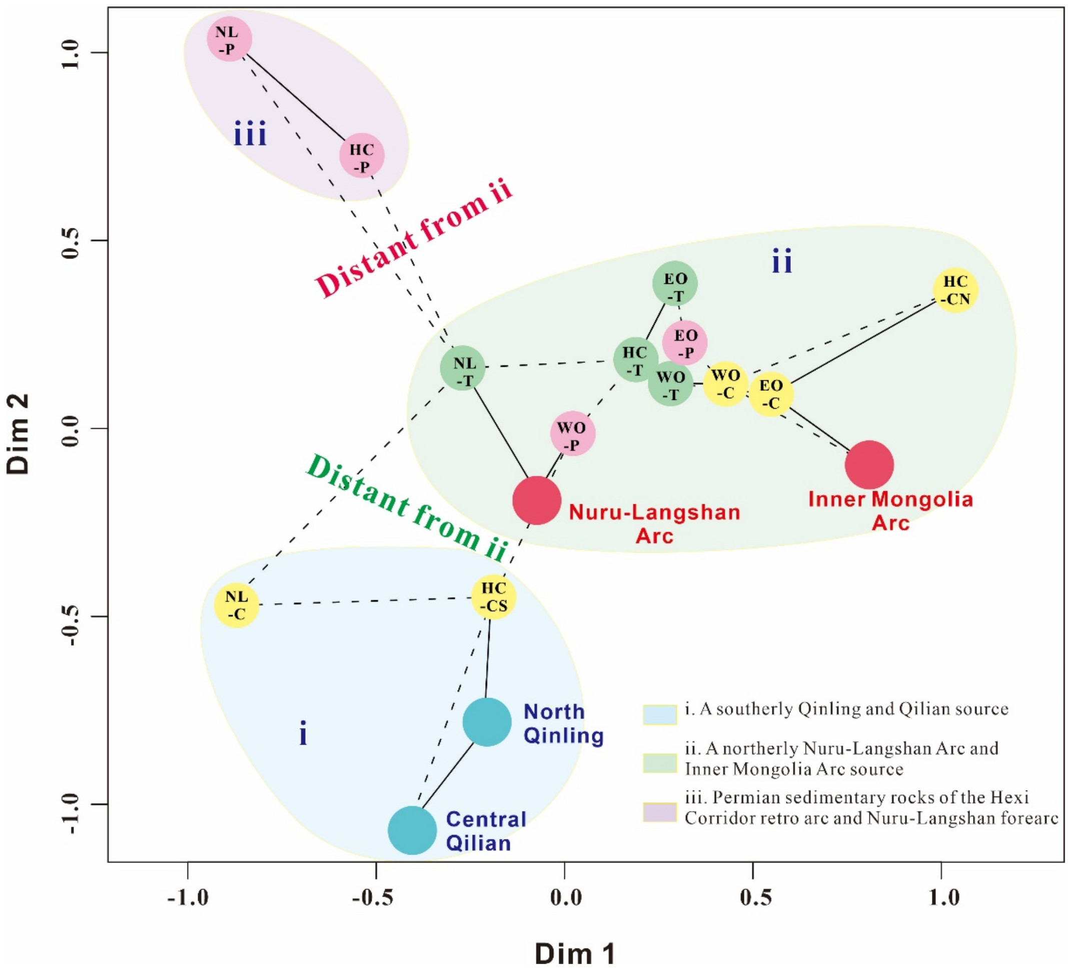

Figure 16. MDS plot of Carboniferous–Triassic strata in the Eastern Hexi Corridor Belt and their potential provenances. Solid and dashed lines indicate the closest and second-closest neighbors, respectively. All plots were generated using the IsoplotR software (http://www.isoplotr.com/isoplotr/).

https://doi.org/10.5194/egusphere-2026-4406
Preprint. Discussion started: 4 September 2026

In summary, in the retroarc and forearc portion of the NLCA, provenances evolved obviously from Carboniferous to Triassic. The Carboniferous sediments in the EHCB retroarc were sourced from erosion of ancient orogens in the Qilian and western NCB, when the forearc was fed by the NLCA basement. Then, the NLCA shed a large volume of Paleozoic arc detritus to the forearc and retroarc portions, before tectonic elevation of the ca. 2700–1700 Ma aged basement materials in Triassic. Throughout the end-Carboniferous to Triassic, sedimentation in the eastern Ordos was dominated by detritus derived from the IMCA, which dispersed a mixing provenance including the ca. 2700–1700 Ma basement and ca. 550–200 Ma arc plutons.

5.2 Paleogeographic evolution of the EHCB and western Ordos Basin

5.2.1 Carboniferous stage

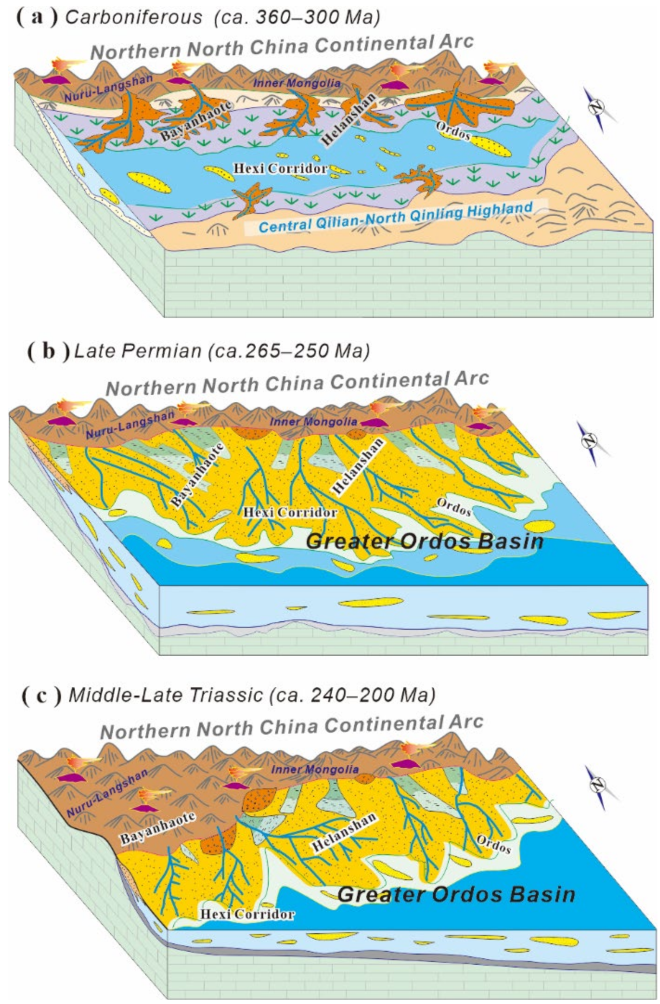

Figure 17. Schematic model showing the polyphase paleogeographic transitions in the Alxa Tectonic Belt, Eastern Hexi Corridor Belt and the Greater Ordos Basin from the Carboniferous to Late Triassic (modified from Sun and Dong, 2020).

https://doi.org/10.5194/egusphere-2026-4406
Preprint. Discussion started: 4 September 2026

In much of the Carboniferous, shallow marine basin was restricted in the EHCB, as there are on time-equivalent strata in the whole western NCB. Ongoing arc extension and crust thinning resulted in rapid transgression and enlargement of basin until late-Carboniferous submergence of the Ordos Basin (Fig. 17a), evident by the ca. 301–297 Ma Benxi Fm (Fig. 3d).

The northerly Qilian-Qinling sources sustained to the earliest Permian from the southern Ordos to the EHCB, fed by mostly ca. 1000–800 Ma and ca. 550–400 Ma with no or rare ca. 350–300 Ma aged detrital zircons (Fig. 15; Yang et al., 2025b). Detrital zircons deposited in the northern EHCB were transported by south-flowing rivers from the nearby western Ordos Basement. Detritus from two opposite sources mingled at the depocenter around the Zhongwei, where Carboniferous strata have the largest thickness of over 2000 m (Tong, 1994).

Sandstones in the northern EHCB show a few ca. 500–300 Ma ages, whereas the Benxi Fm in the northern Ordos comprises numerous Paleozoic zircons (Fig. 14c, d). This view implies that the Paleozoic plutonic bodies in the NLCA have not been elevated then. Hence, the nearby western Ordos supplied most of detrital materials to the northern EHCB. However, at the end-Carboniferous, the whole EHCB and western Ordos were covered by an epeiric sea, sources in the Northern North China Continental Arc further north could be delivered to the basin, as such, the Paleozoic age populations can be detected in most samples.

5.2.2 Permian stage

In the EHCB, Carboniferous marine deposition was punctuated at ca. 295–265 Ma, giving rise to formation of a paraconformity below the Dahuanggou Fm (Fig. 3b). In the Ordos Basin, this sedimentary hiatus was short-lived, lasting from ca. 280 to 260 Ma. (Wu et al., 2021; Shen et al., 2024).

Subsequently, the whole retroarc evolved into continental settings in late Permian, recorded by the Dahuanggou and Yaogou Fms in the EHCB and Shiqianfeng Fm in the northern Ordos. Up to 1000-meter-thick sediments were accumulated in a short time interval of ~15 Ma, defining a compacted rate of ~66 m/Ma that is much higher than ~20 m/Ma for the Carboniferous. Farther to east, accelerated retroarc subsidence was evident by the increasing deposition rate from ~10–20 m/Ma (Yang et al., 2020; Wang et al., 2022b) to ~50–70 m/Ma (Sun et al., 2024) after ca. 280–260 Ma.

Paleocurrent data obtained from southern EHCB strata changes significantly from north- to south-directed, indicating a reversal of drainage system (Fig. 18b). Thick conglomerate beds (Fig. 7e, f) refer to basinward expansion of the continental arc and represent proximal facies of the retroarc EHCB. The previous southerly source in the Central Qilian Orogen has no contribution to the basin, in view of that the whole Central Qilian was submerged by delta and carbonate shelf sequences then (Fig. 17b; Shen et al., 2017), impossible to serve as a source candidate. Age profiles of the EHCB and Central Qilian strata are similar and are characterized by paucity of ca. 1000–600 Ma clusters and enrichment of ca. 500–250 Ma and ca. 2700–1700 Ma ages (He et al., 2024), which are typical age signatures of the NLCA sources.

https://doi.org/10.5194/egusphere-2026-4406
Preprint. Discussion started: 4 September 2026

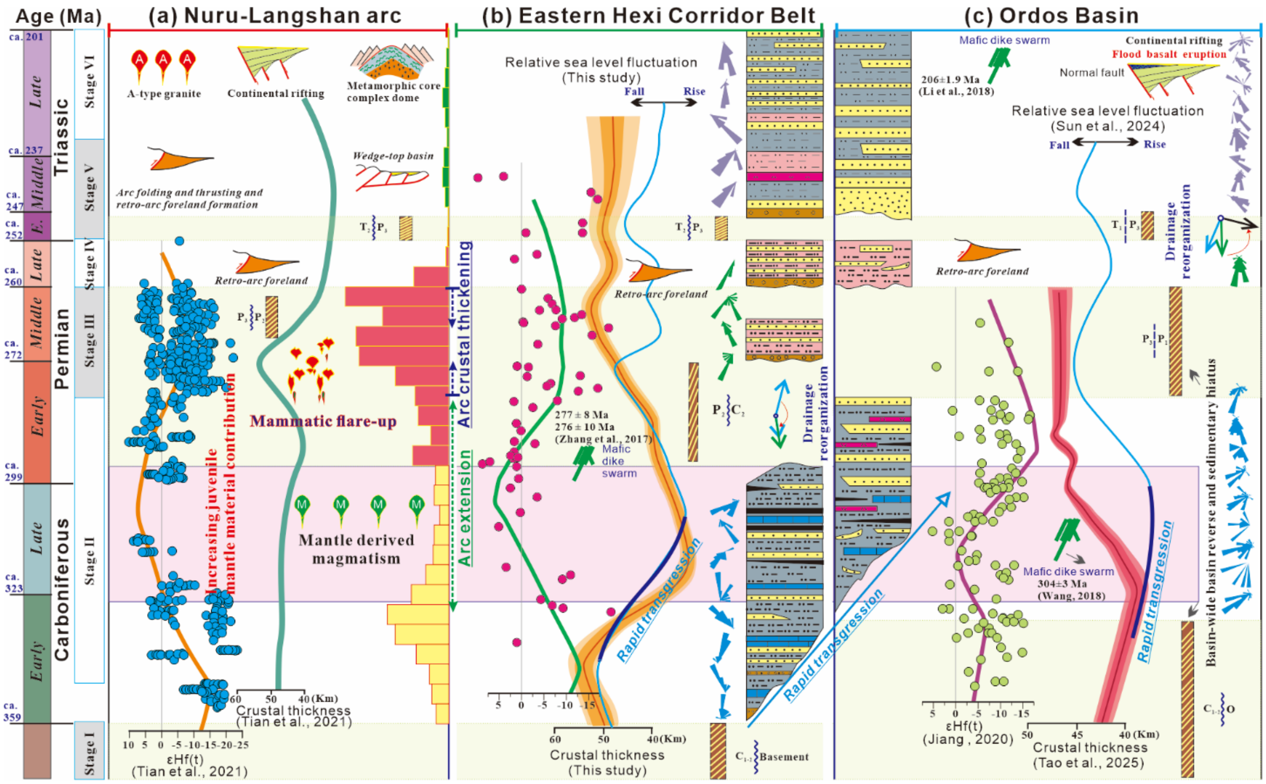

Figure 18. Summary of major Carboniferous to Triassic tectonic events in the Nuru-Langshan Continental Arc, Eastern Hexi Corridor Belt and the Greater Ordos Basin (modified from Sun et al., 2024). See detailed introductions and corresponding references in the main text.

5.2.3 Triassic stage

The Permian, even Carboniferous, units have been intensely deformed and eroded in the northern EHCB (Fig. 3b). Besides the early Triassic depositional hiatus in the retroarc EHCB and northwest Ordos, the most conspicuous chang in paleogeography is a drainage reorganization, as fluvio-delta systems in the northwest Ordos flowed to the southeast (Fig. 17c). For the EHCB, increasing number of ca. 2700–1700 Ma aged detrital zircons in Triassic samples responded to arc thickening and deformation activities. The northern EHCB lacks Permian–Triassic strata (Fig. 3b, c). While provenance analyses reveal that the NLCA derived detrital materials could be transported to the southern EHCB, because samples all contain a swath of 350–250 Ma ages that have no corresponds in the northern EHCB. Thus, the huge Permian–Triassic unconformity represents post-deposition erosion, instead of, simply nondeposition, prior to Early Jurassic deposition (Sun et al., 2024; Yang et al., 2025a).

https://doi.org/10.5194/egusphere-2026-4406
Preprint. Discussion started: 4 September 2026

5.3 Basin evolution and dynamic mechanism of the Andean-type arc-basin system

This work focuses on an Andean-type continental arc and associated basins in the NLCA, EHCB, and western Ordos, aiming to illustrate a multistage paleogeographic evolution model of arc raising and basin shift, and to provide geodynamic forcings from synchronous structural and magmatic expressions in the continental arc.

Ophiolitic mélanges and accretionary complexes in the Engger Us Suture and the Chaganchulu-Tepai Suture, as well as their eastward constitution in the Solonker Suture, indicate existence of the southern PAO basins riming the northern NCB. Zircon U–Pb dating of basalt and gabbro blocks yielded apparent ages of 323±7 to 283±6 Ma, 275±3 Ma, 278±3 Ma, and 279±10 Ma (Miao et al., 2007; Zheng et al., 2014). The chert and siliceous mudstone matrixes contain early-late Permian radiolarian fossils (Song et al. 2024a). Turbidite matrix and sequence associated with the mélange yielded youngest depositional ages of 244±6 Ma from the Engger Us Suture (Song et al., 2024b) and ca. 272–245 Ma from the Solonker Suture (Miao et al., 2007; Fu et al., 2018a). Data of geochronology and biochronology indicate that subduction of the southern PAO lasted to no later than Early Triassic.

5.3.1 Carboniferous to Early Permian arc extension and retroarc rifting

A north-facing continental arc was created upon the western NCB basement from mid-Ordovician (Liu et al., 2016), expressed by pervasive arc magmatism of ca. 458–230 Ma (Xiao et al., 2015; Eizenhöfer and Zhao, 2018; Song et al., 2024b). Slab retreat of the subducting PAO oceanic crust triggered the NLCA extension, ultimately leading to the Quagan Qulu back-arc basin opening in the Carboniferous to early Permian (Song et al., 2024b), recorded by a relative magmatic lull of mantle-derived magmatism with depleted isotopes (Fig. 3a; Liu et al., 2016). The Hf isotopes for arc-derived detrital zircons verify increasing addition of mantle materials (Fig. 18b, c). Crustal thickness estimated from Eu/Eu* reveals an average value of 45±2 km that corresponds to a paleo-elevation of 2 ± 0.2 km for the NLCA (Fig. 19, 20a). The NLCA has not yet been intensely uplifted, and supplied limited detrital materials, as the forearc was dominated by shelf-type carbonate environment (Song et al., 2018). The absence of detrital zircons with ages close to the depositional age (Fig. 15a, b) hint at an extensional tectonic setting for the sedimentation (Cawood et al. 2012).

Ongoing asthenospheric upwelling and thinning of the overlying continental arc (Liu et al., 2016) led to widespread normal faults activities (Luo et al., 2022) and coeval emplacement of diabase sills in the western NCB and EHCB (Wang, 2018; Zhang et al., 2019). In the ECHB, rapid transgression lasted throughout the Carboniferous, given shallow epeiric sea strata continued to onlap towards the Ordos, until late Carboniferous accumulation of the Benxi Fm (Yang et al., 2014; Shen et al., 2018; Ma et al., 2023; Wang et al., 2023b). Due to the low-relief continental arc, moistures from the PAO could be transported to the retroarc interior, resulting in humidification of the NCB (Song et al., 2023; Tao et al., 2025), shown by widespread accumulation of coal-bearing, black-dark gray colored, mudstone deposition (Fig. 6).

https://doi.org/10.5194/egusphere-2026-4406
Preprint. Discussion started: 4 September 2026

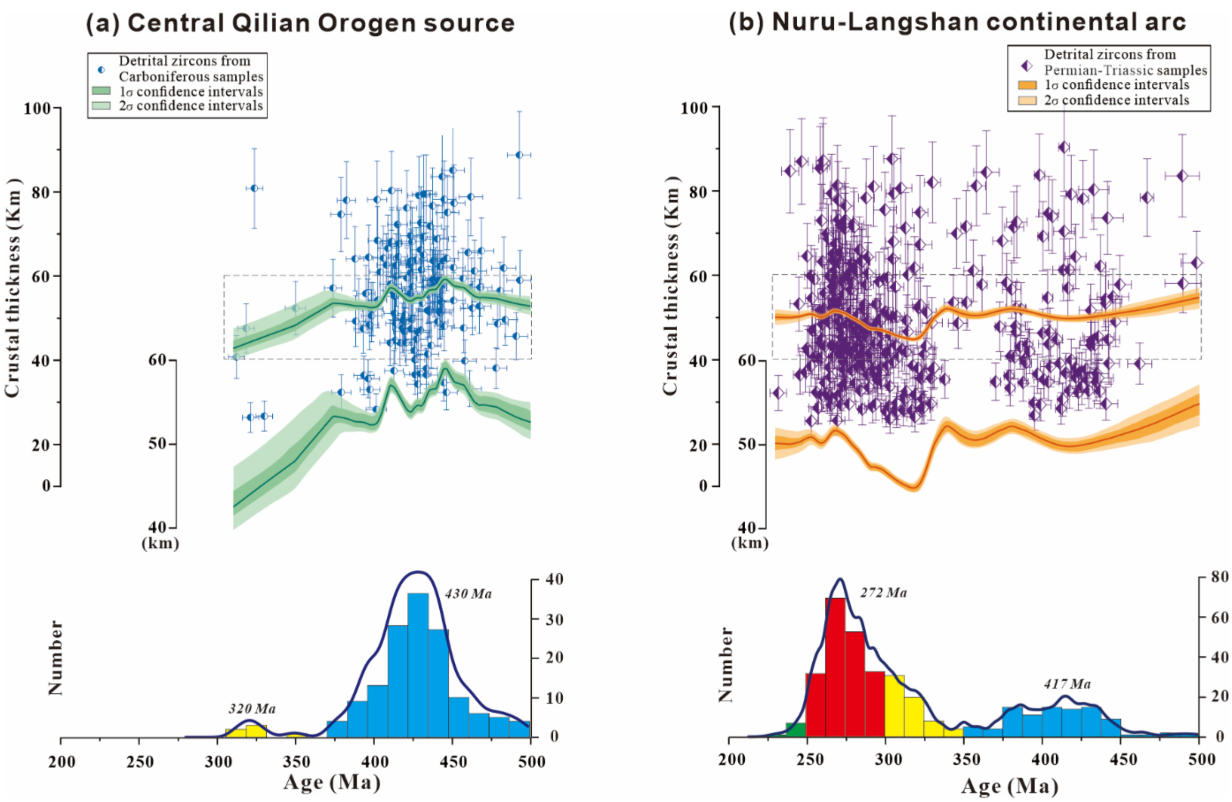

Figure 19. Crustal thickness variation and magmatism fluctuation of the provenance areas reconstructed from Eu/Eu* in Carboniferous and Permian to Triassic detrital zircons from the study area. (a) Detrital zircons sourced from Qilian; (b) Detrital zircons sourced from the Nuru-Langshan continental arc.

5.3.2 Middle-Early Permian arc thickening and retroarc foreland formation

The ca. 278–275 Ma Chaganchulu suprasubduction zone-type ophiolitic mélanges constrain the subduction onset age of the Quagan Qulu Ocean as late as early Permian (Zheng et al. 2014), forming multiple subduction zones in the archipelagic Alxa collage (Song et al., 2024b). The late-stage magmatism of the NLCA commenced in the late Carboniferous and culminated in the Permian (Song et al., 2024b), represented by most of plutons clustering in a relatively short interval of ca. 281–268 Ma (Geng et al., 2007; Dan et al., 2014; Liu et al., 2017; Song et al., 2018, 2020). The mid-Permian igneous rocks display significantly decreasing εHf values (Fig. 18), referring to considerable crustal remelting. The NLCA crust thickened to 55±4 km and corresponding high-relief of 3±0.5 km at mid-Permian (Fig. 20b), consistent within error with 58±11 km thick crust and 3.8±0.7 km paleo-elevation given by Song et al. (2023). This event temporally overlaps with mid-Permian large-scale folding-thrusting (Tian et al., 2020) and ca. 274–268 Ma metamorphism (Liu et al., 2017), reflecting either shallowing of subducting oceanic slab or closure of back-arc basin (Feng et al., 2013; Zheng et al., 2014, 2018; Tian et al., 2020).

https://doi.org/10.5194/egusphere-2026-4406
Preprint. Discussion started: 4 September 2026

The NLCA should be intensely uplifted and eroded at this stage, as Permian strata are rare throughout the NLCA, generating a mid-Permian unconformity in the forearc and intra-arc portions (Song et al., 2018; Tian et al., 2020; Lin et al., 2022), with sources mainly from the Paleozoic arc plutons (Fig. 15a, b). We note that the NLCA-derived samples contain >80% of Paleozoic ages, whereas the IMCA-sourced sediments have considerable Precambrian aged zircons. We assume that the Paleozoic plutonic bodies, in particular Permian intrusions, in the NLCA have been intensely and rapidly elevated, and that the Northern North China Continental experienced a diachronous uplift history during Permian.

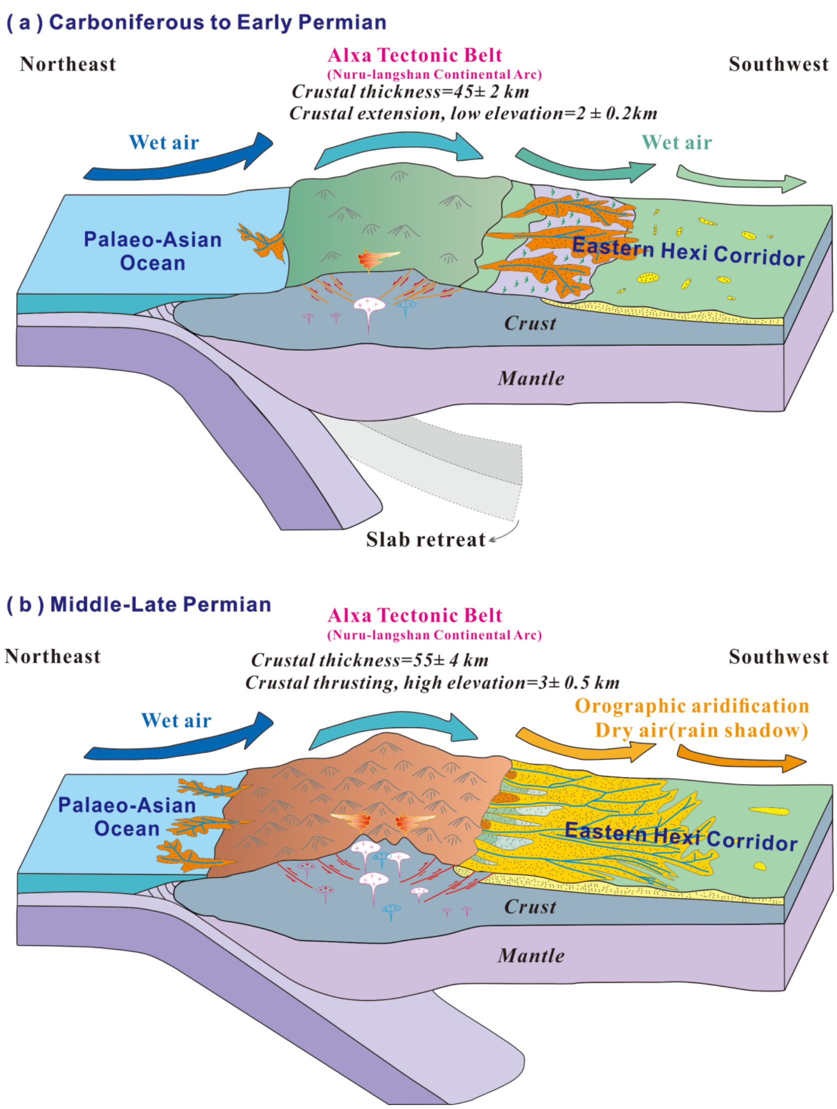

Figure 20. Tectonic evolution, paleogeographic transition, and sediment provenance changing in the Nuru-Langshan Continental Arc and Eastern Hexi Corridor Retro Arc (Tao et al., 2025). The calculation of crust thickness and altitude is based on Tang et al. (2020, 2024) (a) Carboniferous to early Permian; (b) middle to late Permian.

Ongoing crustal thickening and top-to-the-S thrusting in the NLCA (Zhang et al., 2013; Tian et al., 2020) induced formation of a craton-wide mid-Permian unconformity that represents a mid-Permian deposition hiatus in the retroarc EHCB and Ordos Basin (Wu et al., 2021; Shen et al., 2021, 2022). The Late Permian retroarc foreland system extended from wedge-top in the NLCA, represented by the Dahongshan Fm (Lin et al., 2022), to the retroarc EHCB and Ordos Basin, characterized by increasing deposition rate from ~10–20 m/Ma to ~50–70 m/Ma (Yang et al., 2020; Sun et al., 2024) after mid-Permian. The 3±0.5 km high-relief NLCA is comparable to the elevation of the present-day Andes (Song et al., 2023). The orographic barrier hindered moisture transportation from the ocean to the retroarc portion and triggered aridification in the EHCB and the western NCB (Fig. 20b; Cope et al., 2005; Song et al., 2023; Sun et al., 2024; Tao et al., 2025), expressed by late Permian red-bed mudstone deposition (Fig. 3 and 7).

5.3.3 Triassic arc outgrowth and syn-orogenic retroarc drainage reorganization

Identification of juvenile Mongolian arcs detritus in Ladinian-Carnian strata of the NLTB constrains closure of the PAO in the Alxa at ca. 242–233 Ma (Song et al., 2024b). Coeval provenance exchange also has been found in the Solonker Suture (Song et al., 2024a). The shift coincided with extensive ca. 255–230 Ma metamorphism in the NLCA (Li et al., 2017; Yan et al., 2022), which was displaced southwestwards for 160–180 km by the Bayanwula Fault then (Zhang et al., 2013, 2022). The NLCA outgrowth event was followed by intense basin reversal in the Bayanhaote Basin and shrinkage of the Greater Ordos Basin subsequently (Fig. 17c).

In the southern CAOB, widespread eastward extrusions (Wang et al., 2008, 2011) resulted in eastward outgrowth of the thickened NLTB, represented by uplift and erosion of the nearby Bayanhaote Basin and an Early Triassic unconformity in the EHCB and western Ordos Basin (Fig. 18). Sun et al. (2024) reported up to 1 m-long sandstone gravels in the western Helanshan and advocated it as evidence for the NLCA highland expansion toward basin, which led to sediment recycling of Paleozoic strata. Sandstone gravels show an age profile (Fig. 15d) distinct from a NLCA source, but, similar to ages of Ordovician turbidites in the Bayanhaote Basin (Sun et al., 2024).

The Mid- to Late Triassic synorogenic sediments in the NLCA were demonstrated and were explained to be formed in syn-orogenic retro-arc foreland basin (Song et al. 2024a). At the beginning of Middle Triassic, a craton-scale drainage reorganization was promoted, given that fluvial-delta systems began to discharge to the southeast (Fig. 18c). As crustal thickening intensified, the NLCA supplied increasing amounts of basement material to the retroarc foreland, as indicated by abundant ca. 2700-1700 Ma detrital zircons in Triassic sandstone samples from the EHCB. The paucity of ca. 1500-400 Ma zircons further suggests that the NLCA occupied the highest relief in the southern CAOB, which restricted the transport of Mesoproterozoic Mongolian arc detritus into the retroarc interior.

https://doi.org/10.5194/egusphere-2026-4406
Preprint. Discussion started: 4 September 2026

6 Conclusions

New sedimentological and provenance data, together with existing geological observations, support the following conclusions:

(1). The youngest 8 ages define a weighted mean age of 268±3 Ma for the basal Dahuanggou Fm, constraining its deposition age to be no older than mid-Permian. The Yaogou Fm samples contain a number of zircons younger than ca. 260 Ma, constraining age of the Yaogou Fm to be Late Permian.

(2). Two basin transition and paleodrainage reorganization events at ca. 295–265 Ma and ca. 250–240 Ma subdivide evolution history of the western Ordos and EHCB into 3 stages, i.e., Carboniferous retroarc extension stage, middle-late Permian retroarc foreland basin stage, and middle-late Triassic syn-collision stage.

(3). The Carboniferous strata in the southern EHCB were sourced from the Central Qilian terrane and contain mainly Paleozoic and Neoproterozoic detrital zircons. In contrast, northern EHCB samples are dominated by ca. 2700-1700 Ma ages, indicating derivation from the Ordos basement. Crustal thinning, normal faulting, and mantle-derived magmatism together indicate an extensional setting.

(4). The middle-late Permian strata were fed by younger arc plutons in the NLCA, given >80% number of Paleozoic-age zircons in forearc and retroarc sediments. Crustal thickening and negative ε(Hf) values refer to an intensely raising NLCA, cratonward expansion of which built a retroarc foreland system in the western Ordos and EHCB. The ~3±0.5 km high relief of the IMCA triggered orographic rain shadow and retroarc aridification, indicated by changing of mudstone color from black to red.

(5). Early Triassic PAO closure enhanced uplift of the NLCA basement and left-lateral strike-slip motion along the Bayanwula Fault, supplying ca. 2700-1700 Ma detrital zircons to the retroarc. Paleodrainage was reorganized at the same time, as western Ordos fluvial-deltaic systems began to route sediment southeastward.

(6). Sedimentary fluctuation of the EHCB dynamically coincided with changing tectonic regime of the NLCA, revealing an evolving Andean-type retroarc basin system during the PAO termination.

Appendices

1. Sampling and analytical methods

1.1. Paleocurrent reconstruction

During field investigations, orientations of paleocurrent indicators, including medium- to large- scaled cross-beddings and pebble imbrications, were measured from Carboniferous, Permian, and Triassic outcrops. Measurement results are listed in Supplementary Table 2. After tilt restoration, the reconstruct paleoflow directions are illustrated by rose diagrams (Fig. 2b).

1.2. Sandstone petrology and detrital modal analysis

https://doi.org/10.5194/egusphere-2026-4406
Preprint. Discussion started: 4 September 2026

Sandstone petrologic studies were conducted on 30 sandstone samples, including 10 Carboniferous samples, 12 Permian samples, and 8 Triassic samples. The principal particle types were determined using an optical microscope. Point-counting was carried out under direction of the Gazzi-Dickinson point-counting method (Dickinson and Suczek 1979; Ingersoll et al. 1984). A minimum of 450 grains were counted on each sample. The full list of data can be found in Supplementary Table 3, and the representative photomicrographs are labeled in Supplementary Fig. 1. Framework grains were classified into quartz (Q), including monocrystalline quartz (Qm) and polycrystalline quartz (Qp); feldspar (F); and unstable lithic fragments (L), comprising metamorphic (Lm), volcanic (Lv), and (meta)sedimentary (Ls) types. The statistical results were plotted on Qt–F–L, Qm–F–Lt, and Qp–Lv–Ls ternary diagrams to illustrate the tectonic setting of the source terranes (Fig. 9).

1.3. Detrital zircon U-Pb LA-ICP-MS geochronology

Four Carboniferous samples, three Permian samples, and four Triassic samples were analyzed by laser ablation–inductively coupled plasma–mass spectrometry (LA-ICP-MS) zircon U-Pb geochronological studies at Northwest China Center for Geoscience Innovation. Analytical procedures follow Liu et al. (2007b), including instrument parameters, experimental protocols, and data processing. Sample location, stratigraphic level, and petrology are summarized in Supplementary Table 4. Complete detrital zircon U–Pb datasets are listed in Supplementary Table 5 and representative CL images are shown in Supplementary Fig. 2. The206Pb/238U age is used for zircons younger than 1000 Ma, whereas the207Pb/206Pb age is used for zircons older than 1000 Ma (Black et al., 2003). All analytical results are plotted on concordia diagrams, and analyses exceeding 10% discordance were excluded from frequency diagrams (Fig. 10–12).

1.4. In-situ Lu-Hf isotope

The in-situ Lu-Hf isotope analysis of zircon microregions was conducted in the Key Laboratory of Continental Dynamics of Northwest University. The laser ablation system is a 193nm molecular laser ablation system (RESOlution M-50, ASI), which includes a 193nm ArF molecular laser, a dual-chamber sample chamber, and a computer-controlled high-precision X-Y sample stage movement and positioning system. The dual-chamber sample cell can effectively avoid cross-contamination between samples, reduce sample blowing time, and significantly increase the loading capacity of samples, thereby reducing the influence of human factors during frequent sample changes. During the analysis process, the international standard zircon samples GJ-1 and Mudtank were used as monitoring samples. Every 10 samples were inserted into a group of international standard samples. The data acquisition mode was TRA mode, with an integration time of 0.2s, a background acquisition time of 30s, a sample integration time of 45s, and a blowing time of 40s. The detailed analysis method and instrument parameters can be found in Bao et al., 2023. In-situ Lu-Hf isotope results of detrital zircons with U-Pb ages of ca. 500–200 Ma are presented by Supplementary Table 6.

https://doi.org/10.5194/egusphere-2026-4406
Preprint. Discussion started: 4 September 2026

Data availability

All data related to this work are provided in the Supplement and will be available online together with the published article.
Supplementary Table 1:
https://docs.google.com/spreadsheets/d/1dTWhaQE9M6oIAf-DkOyiY7OtqKlVWVmDchcHSC__ExI/edit?usp=sharing
Supplementary Table 2:
https://docs.google.com/spreadsheets/d/1DTrqsINCEhv4xsPihIkDncrFcB5YJcVIP_HCsPW3tBw/edit?usp=sharing
Supplementary Table 3:
https://docs.google.com/spreadsheets/d/1FXT6aaa-q0fWbECezk6mTcCr8vTIYC6BrZW3-XBUAbk/edit?usp=sharing
Supplementary Table 4:
https://docs.google.com/spreadsheets/d/1oOsSgMp-Nh7u6Q64nd-ZonWyoKmVYCXVzaD8XrnXYvw/edit?usp=sharing
Supplementary Table 5:
https://docs.google.com/spreadsheets/d/14mmhZvMBvUj4PlYVL0edR5yhGPP-EioB4d5yDbkfzMA/edit?usp=sharing
Supplementary Table 6:
https://docs.google.com/spreadsheets/d/1EGhZ-V3-rfRDlvPfe_xG0WiQBnVXLZpuQH1qhjJxmsA/edit?usp=sharing

Author contributions

Junxiang Zhang: Writing-original draft, Visualization, Investigation, Methodology, Formal analysis, Data curation. **Jiaopeng Sun:** Writing-review & editing, Supervision, Investigation, Formal analysis, Data curation, Funding acquisition. **Yunpeng Dong:** Writing-review & editing, Conceptualization, Formal analysis. **Xiaofeng Han:** Writing-review & editing, Investigation, Formal analysis. **Xiangyang, Yang:** Writing-review & editing, Investigation, Formal analysis. **Yukun Qi:** Writing-review & editing, Investigation.

Competing interest

The authors declare that they have no known competing financial interests or personal relationships that could have appeared to influence the work reported in this paper.

Acknowledgements

The authors acknowledge editors and referees for insightful comments that led to a better version of our work. Financial support was jointly given by the National Natural Science Foundation of China (Grants: 42372253 and 42072260), the Youth

https://doi.org/10.5194/egusphere-2026-4406
Preprint. Discussion started: 4 September 2026

Innovation Team of Shaanxi Universities, and Science and Technology Project of PetroChina (Nos. 2023ZZ0201 and 2024D1JC06).

References

Bao, Z., Chen, K., Kang, L., Zong, C., Nie, X., Lv, N., and Yuan, H.: Comparison of synthetic zircon, high-temperature and high-pressure sintered zircon and fast hot-pressing sintered zircon for in situ hafnium isotope analysis by LA-MC-ICP-MS. J Anal Atom Spectrom, 38(11), 2313-2323. https://doi.org/10.1039/D3JA00137G, 2023.

Black, L. P., Kamo, S. L., Allen, C. M., Aleinikoff, J. N., Davis, D. W., Korsch, R. J., and Foudoulis, C.: TEMORA 1: a new zircon standard for Phanerozoic U–Pb geochronology. Chemical geology, 200(1-2), 155-170. https://doi.org/10.1016/S0009-2541(03)00165-7, 2003.

Boschman, L. M.: Andean mountain building since the Late Cretaceous: A paleoelevation reconstruction. Earth-Sci Rev. 220, 103640. https://doi.org/10.1016/j.earscirev.2021.103640, 2021.

Cawood, P.A., Hawkesworth, C.J., and Dhuime, B.: Detrital zircon record and tectonic setting. Geology, 40(10), 875-878. https://doi.org/10.1130/G32945.1, 2012.

Chen, S., Guo, Z., Qi, J., Zhang, Y., Pe-Piper, G., Piper, D.J.W.: Early Permian volcano-sedimentary successions, Beishan, NW China: Peperites demonstrate an evolving rift basin. J. Volcanol. Geotherm. Res. 309, 31–44. https://doi.org/10.1016/j.jvolgeores.2015.11.004, 2016.

Cohen, K. M., Finney, S. C., Gibbard, P. L., and Fan, J. X.: The ICS international chronostratigraphic chart. Episodes Journal of International Geoscience, 36(3), 199-204. https://doi.org/10.18814/epiiugs/2013/v36i3/002, 2013.

Cope, T., Ritts, B., Darby, B., Fildani, A., and Graham, S.: Late Paleozoic sedimentation on the northern margin of the North China block: Implications for regional tectonics and climate change. Int Geol Rev, 47(3), 270-296. https://doi.org/10.2747/0020-6814.47.3.270, 2005.

Dan, W., Li, X.H., Wang, Q., Wang, X.C., and Liu, Y.: Neoproterozoic S-type granites in the Alxa Block, westernmost North China, and tectonic implications: In situ zircon U-Pb-Hf-O isotopic and geochemical constraints. Am J Sci, 314(1), 110-153. https://doi.org/10.2475/01.2014.04, 2014.

DeCelles, P. G., Ducea, M. N., Kapp, P., and Zandt, G.: Cyclicity in Cordilleran orogenic systems. Nat Geosci, 2(4), 251-257. https://doi.org/10.1038/ngeo469, 2009.

DeCelles, P. G., and Graham, S. A.: Cyclical processes in the North American Cordilleran orogenic system. Geology, 43(6), 499-502. https://doi.org/10.1130/G36482.1, 2015.

Deng, S., Lu, Y., Luo, Z., Fan, R., Li, X., Zhao, Y., and Cui, J.: Subdivision and age of the Yanchang Formation and the Middle/Upper Triassic boundary in Ordos Basin, North China. . Sci China Earth Sci, 61(10), 1419-1439. https://doi.org/10.1007/s11430-017-9215-3, 2018.

https://doi.org/10.5194/egusphere-2026-4406
Preprint. Discussion started: 4 September 2026

Dickinson, W. R.: Provenance and sediment dispersal in relation to paleotectonics and paleogeography of sedimentary basins. New perspectives in basin analysis. New York, NY: Springer New York, 1988. 3-25. https://doi.org/10.1007/978-1-4612-3788-4_1, 1988.

Dickinson, W. R., and Suczek, C. A.: Plate tectonics and sandstone compositions. Aapg Bulletin, 63(12), 2164-2182. https://doi.org/10.1306/2F9188FB-16CE-11D7-8645000102C1865D, 1979.

Ding, X., and Lithgow-Bertelloni, C.: Retroarc foreland basins document past oceanic subduction history. Earth Planet Sc Lett, 663, 119412. https://doi.org/10.1016/j.epsl.2025.119412, 2025.

Dong, Y., Sun, S., Santosh, M., Zhao, J., Sun, J., He, D., Shi, X., Hui, B., Cheng, C., Zhang, G.: Central China Orogenic Belt and amalgamation of East Asian continents. Gondwana Res. 100, 131–194. https://doi.org/10.1016/j.gr.2021.03.006, 2021.

Du, B.A.: Middle Triassic Palynological assemblage in the Wangjiashan Basin of Jingyuan, Gansu and Its Stratigraphical Significance. J Integr Plant Biol, 27(5) (in Chinese with English abstract), 1985.

Eizenhöfer, P.R.: Subduction and Closure of the Pal- aeo-Asian Ocean along the Solonker Suture Zone: Con- straints from an Integrated Sedimentary Provenance Analysis. Singapore, Springer, 270 p. https://doi.org/10.1007/978-981-32-9200-0, 2019.

Eizenhöfer, P. R., and Zhao, G.: Solonker Suture in East Asia and its bearing on the final closure of the eastern segment of the Palaeo-Asian Ocean. Earth-Sci Rev, 186, 153-172. https://doi.org/10.1016/j.earscirev.2017.09.010, 2018.

Eizenhöfer, P.R., Zhao, G.C., Zhang, J., and Sun, M.: Final closure of the Paleo-Asian Ocean along the Solonker suture zone: Constraints from geochronological and geochemical data of Permian volcanic and sedimentary rocks. Tectonics, 33(4), 441-463. https://doi.org/10.1002/2013TC003357, 2014.

Eizenhöfer, P.R., Zhao, G.C., Sun, M., Zhang, J., Han,Y.G., and Hou, W.Z.: Geochronological and Hf isotopic variability of detrital zircons in Paleozoic strata across the accretionary collision zone between the North China craton and Mongolian arcs and tectonic implications. Bulletin, 127(9-10), 1422-1436. https://doi.org/10.1130/B31175.1, 2015.

Fang, Q., Gao, J. H., Wang, X. L., and Jing, X. C.: The Carboniferous–Permian conodont succession in the North Qilian Mountain region. Acta Palaeontol Sin, 53, 363-380 (in Chinese with English abstract), 2014.

Feng, J.Y., Xiao, W.J., Windley, B., Han, C.M., Wan, B., Zhang, J.E., Ao, S.J., Zhang, Z.Y., and Lin, L.N.: Field geology, geochronology and geochemistry of mafic-ultramafic rocks from Alxa, China: Implications for late Permian accretionary tectonics in the southern Altaids. J Asian Earth Sci, v. 78, p. 114–142. https://doi.org/10.1016/j.jseaes.2013.01.020, 2013.

Fu, D., Huang, B., Kusky, T.M., Li, G., Wilde, S.A., Zhou, W., Yu, Y.: A middle Permian ophiolitic mélange belt in the Solonker suture zone, western Inner Mongolia, China: Implications for the evolution of the Paleo-Asian Ocean. Tectonics 37 (5), 1292–1320. https://doi.org/10.1029/2017TC004947, 2018a.

Fu, C.L., Yan, Z., Guo, X.Q., Niu, M.L., Cao, B., Wu, Q., Li, X.C., and Wang, Z.Q.: Assembly and dispersal history of continental blocks within the Altun-Qilian-North Qaidam mountain belt, NW China, International Geology Review, 61(4), 424-447. https://doi.org/10.1080/00206814.2018.1428831, 2018b.

https://doi.org/10.5194/egusphere-2026-4406
Preprint. Discussion started: 4 September 2026

Fu, C.L., Yan, Z., Aitchison, J.C., Xiao, W.J., Buckman, S., Wang, B.Z., Li, W.F., Li, Y.S., and Ren, H.D.: Multiple subduction processes of the Proto-Tethyan Ocean: Implication from Cambrian intrusions along the North Qilian suture zone, Gondwana Res, 87, 207–223. https://doi.org/10.1016/j.gr.2020.06.007, 2020.

Fu, C.L., Yan, Z., Aitchison, J.C., Xiao, W.J., Buckman, S., and Wang, B.Z.: Subduction Within the Proto-Tethys Ocean Revealed by Recognition of the Earliest Phanerozoic Intra-Oceanic Arc, Northern Tibetan Plateau. Earth Space Sci, 11(3), e2023EA002985. https://doi.org/10.1029/2023EA002985, 2024.

Garzanti, E., Capaldi, T., Tripaldi, A., Zárate, M., Limonta, M., and Vezzoli, G.: Andean retroarc-basin dune fields and Pampean Sand Sea (Argentina): Provenance and drainage changes driven by tectonics and climate. Earth-Sci Rev, 231, 104077. https://doi.org/10.1016/j.earscirev.2022.104077, 2022.

Geng, Y.S., Wang, X.S., Shen, Q.H., and Wu, C.M.: Chronology of the Precambrian metamorphic series in the Alxa area, Inner Mongolia. Geology in China, 34(2), 251-261 (in Chinese with English abstract). https://doi.org/CNKI:SUN:DIZI.0.2007-02-006, 2007.

Guo, Y.Q., Li, W.H., Guo, C.B., Zhang, Q., Chen, Q., Wang, R.G., Liu, X., Ma, Y., Li, Z.C., Zhang, M.T., and Li, B.Q.: Sedimentary systems and palaeogeography evolution of Ordos Basin. J. Palaeogeogr., 21(2), 293-320 (in Chinese with English abstract). https://doi.org/10.26914/c.cnkihy.2021.016540, 2019.

He, W., Sun, J., Dong, Y., Qian, T., Wang, T., He, L., and Qi, Y.: A synthesis of available detrital zircon data from the Qilian-Qaidam-Kunlun collage, northern Tibet. Geosci Data J, 11(4), 465-478. https://doi.org/10.1002/gdj3.225, 2024.

Ingersoll, R. V., Bullard, T. F., Ford, R. L., Grimm, J. P., Pickle, J. D., and Sares, S. W.: The effect of grain size on detrital modes: a test of the Gazzi-Dickinson point-counting method. J Sediment Res, 54(1), 103-116. https://doi.org/10.1306/212F83B9-2B24-11D7-8648000102C1865D, 1984.

Jahn, B.M., Windley, B., Natal'in, B., Dobretsov, N.: Phanerozoic continental growth in Central Asia. J. Asian Earth Sci. 23, 599–603. https://doi.org/10.1016/S1367-9120(03)00124-X, 2004.

Kou, L.L., Li, H.L., Li, Z.H., Dond, X.P, Cui, J.W., Huang, T.: Sedimentary age and provenance tracing of the Permian Hongquan Formation in the Yantongshan structural belt on the northeastern margin of the Qinghai-Xizang Plateau. Geological Bulletin of China, 41(2-3): 315-326 (in Chinese with English abstract). https://doi.org/10.12097/j.issn.1671-2552.2022.2-3.011, 2022.

Li, W. H., Pang, J. G., Cao, H. X., Xiao, L., and Wang, R. G.: Depositional system and paleogeographic evolution of the late Triassic Yanchang Stage in Ordos Basin. J. Northwest A&F Univ. (Nat. Sci. Ed.), 39(3), 501-506. https://doi.org/CNKI:SUN:XBDZ.0.2009-03-022, 2009.

Li, S., Chung, S.L., Wilde, S.A., Jahn, B.M., Xiao, W.J., Wang, T., and Guo, Q.Q.: Early–Middle Triassic high Sr/Y granitoids in the southern Central Asian Orogenic Belt: Implications for ocean closure in accretionary orogens. J. Geophys. Res., Solid Earth, 122(3), 2291-2309. https://doi.org/10.1002/2017JB014006, 2017.

Li, Z.H.: Paleozoic tectonic evolution in the Helanshan Tectonic Belt: constraints from U-Pb geochronology of detrital zircon. Ph. D. thesis, 94. 2018.

https://doi.org/10.5194/egusphere-2026-4406
Preprint. Discussion started: 4 September 2026

Li, W.H., Liu, X., Zhang, Q., Guo, Y.Q., Li, K.Y., Yuan, Z., Wang, Y., Ma, Y., Bai, J.L., Yang, B., and Li, Z.Y.: Deposition evolution of Middle–Late Triassic Yanchang Formation in Ordos Basin. J. Northwest A&F Univ. (Nat. Sci. Ed.). 49(4), 605-621(in Chinese with English abstract). https://doi.org/10.16152/j.cnki.xdxbzr.2019-04-013, 2019.

Li, Y., Wang, X. D., Hu, K. Y., Huang, X., Zhang, S. C., Zhang, B., and Yao, L.: Lithostratigraphic subdivision and correlation of the Carboniferous in China. Journal of Stratigraphy, 45(3), 303-318. https://doi.org/10.19839/j.cnki.dcxzz.2021.0026, 2021.

Lin, C.N., Xie, G.A., Tian, R.S., Wang, B., and Zhang, Q.L.: The age and potential provenance information of Dahongshan Formation in the Langshan, the north-eastern margin of the Alxa block and its geological implications. Geological Review (Dizhi Lunping), 68, 781-796 (in Chinese with English abstract). https://doi.org/10.16509/j.georeview.2022.01.051, 2022.

Liu, X., Gao, S., Diwu, C., Yuan, H., and Hu, Z.: Simultaneous in-situ determination of U-Pb age and trace elements in zircon by LA-ICP-MS in 20 μm spot size: Chinese Science Bulletin, 52(9). 1257–1264. https://doi.org/10.1007/s11434007-0160-x, 2007.

Liu, Q., Zhao, G.C., Sun, M., Han, Y.G., Eizenhöfer, P.R., Hou, W.Z., Zhang, X.R., Zhu, Y.L., Wang, B., Liu, D.X., and Xu, B.: Early Paleozoic subduction processes of the Paleo-Asian Ocean: Insights from geo-chronology and geochemistry of Paleozoic plutons in the Alxa terrane. Lithos, 262, 546-560. https://doi.org/10.1016/j.lithos.2016.07.041, 2016.

Liu, Q., Zhao, G.C., Han, Y.G., Eizenhöfer, P.R., Zhu, Y.L., Hou, W.Z., Zhang, X.R., and Wang, B.: Geochronology and geochemistry of Permian to Early Triassic granitoids in the Alxa terrane. Constraints on the final closure of the Paleo-Asian Ocean. Lithosphere, 9(4), 665-680. https://doi.org/10.1130/L646.1, 2017.

Liu, J., Sun, J., Chen, Q., Kou, F., Ma, Y., Wang, T. and Qi, Y.: Late Paleozoic Accumulation of Coal-Bearing Successions in the Wuhai Coalfield, Western North China: Back-Arc Basin Response to Southward Subduction of the Paleo-Asian Ocean. Energies, 16(1), 34. https://doi.org/10.3390/en16010034, 2022.

Liu, M., Lai, S. C., Ma, S., Zhang, F. Y., Zhu, R. Z., Zhu, Y. and Yang, H.: An enhanced chemical maturation of juvenile arc crust recorded by the Urad Houqi intrusive suite in Langshan arc, Central Asia. Geol Soc Am Bull, 136(11-12), 4616-4632. https://doi.org/10.1130/B37465.1, 2024.

Luo, G.C. and Wang, M.Z.: New Knowledge On The Study Of The Early Permian Stratigraphy In the eastern part of the Hexi Corridor Region. J. Earth Sci. Environ., (02): 16-25 (in Chinese with English abstract), 1992.

Luo, C.Y., Song, L.J., Yang, H., Shi, C.Y., and Zhang, H.: Tectonic evolution and thermal history simulation of Ermahu Sag, Wuwei Basin. Northwest. Geol., 55(4), 194-203. https://doi.org/10.19751/j.cnki.61-1149/p.2022.04.017, 2022.

Ma, R., Yang, J., Wang, Y., Yan, J., and Liu, J.: Estimating the magnitude of early Permian relative sea-level changes in southern North China. Global Planet Change, 221, 104036. https://doi.org/10.1016/j.gloplacha.2023.104036, 2023.

Ma, X.C., Liu, L., Wang, Z.W.: Detrital Material Source and Paleogeographic Reconstruction of Taiyuan Formation in Western Ordos Basin. Acta Sedimentol. Sin. (in Chinese with English abstract). https://doi.org/10.14027/j.issn.1000-0550.2024.134, 2025.

Mason, E., Edmonds, M., and Turchyn, A. V.: Remobilization of crustal carbon may dominate volcanic arc emissions. Science, 357(6348), 290-294. https://doi.org/10.1126/science.aan5049, 2017.

https://doi.org/10.5194/egusphere-2026-4406
Preprint. Discussion started: 4 September 2026

McKenzie, N. R., Horton, B. K., Loomis, S. E., Stockli, D. F., Planavsky, N. J. Lee, C. T. A.: Continental arc volcanism as the principal driver of icehouse-greenhouse variability. Science, 352(6284), 444-447. https://doi.org/10.1126/science.aad5787, 2016.

Miao, L.C., Zhang, F.Q., Fan, W.M., Liu, D.Y.: Phanerozoic evolution of the Inner Mongolia-Daxinganling orogenic belt in North China: Constraints from geochronology of ophiolites and associated formations. Geol. Soc. Lond. Spec. Publ. 280 (1), 223–237. https://doi.org/10.1144/SP280.11, 2007.

Montañez, I. P., McElwain, J. C., Poulsen, C. J., White, J. D., DiMichele, W. A., Wilson, J. P., and Hren, M. T.: Climate, p CO2 and terrestrial carbon cycle linkages during late Palaeozoic glacial–interglacial cycles. Nat Geosci, 9(11), 824-828. https://doi.org/10.1038/ngeo2822, 2016.

Peng, H., Ding, L., Liu, C., Zattin, M., Wang, J., and Wang, L.: Middle Triassic transcontinental connection between the North China Craton and the Paleo-Tethys Ocean. Commun Earth Environ, 5(1), 775. https://doi.org/10.1038/s43247-024-01945-z, 2024.

Peng, Y., Yu, S., Li, S., Zhang, J., Liu, Y., Li, Y., and Santosh, M.: Early Neoproterozoic magmatic imprints in the Altun-Qilian-Kunlun region of the Qinghai-Tibet Plateau: Response to the assembly and breakup of Rodinia supercontinent. Earth-Sci Rev, 199, 102954. https://doi.org/10.1016/j.earscirev.2019.102954, 2019.

Plank, T., and Manning, C. E.: Subducting carbon. Nature, 574(7778), 343-352. https://doi.org/10.1038/s41586-019-1643-z, 2019.

Qu, H.J., Han, X., Chen, S., and Yang, B.: U-Pb dating of detrital zircon from the upper paleozoic clastic rocks and basin-mountain coupling of the northeastern Ordos Basin. Geotecton. Metallog, 44, 501-527. https://doi.org/10.16539/j.ddgzyckx.2020.03.013, 2020.

Şengör, A. C., Natal'in, B. A., Sunal, G., and van der Voo, R.: The tectonics of the Altaids: Crustal growth during the construction of the continental lithosphere of Central Asia between□750 and□130 Ma ago. Annu Rev Earth Pl Sc, 46(1), 439-494. https://doi.org/10.1146/annurev-earth-060313-054826, 2018.

Shen, W., Shao, L., Tian, W., Sun, B., Chen, G., Chen, F., and Lu, J.: Sequence stratigraphy, palaeogeography, and coal accumulation in a gently sloping paralic basin: A case study from the Carboniferous–Early Permian Wuwei Basin, northwestern China. Geological Journal, 53(5), 2386-2412. https://doi.org/10.1002/gj.3123 , 2018.

Shen, B. H., Shen, S. Z., Hou, Z. S., Wu, Q., Zhang, S. C., Zhang, B., and Yuan, D. X.: Lithostratigraphic subdivision and correlation of the Permian in China. Journal of Stratigraphy, 45(3), 319-339 (in Chinese with English abstract). https://doi.org/10.19839/j.cnki.dcxzz.2021.0027, 2021.

Shen, B. H., Shen, S., Wu, Q., Zhang, S., Zhang, B., Wang, X., and Feng, Z.: Carboniferous and Permian integrative stratigraphy and timescale of North China Block. Sci China Earth Sci, 65(6), 983-1011. https://doi.org/10.1007/s11430-021-9909-9, 2022.

Shen, B. H., Hou, Z. S., Wang, X. D., Wu, Q., Zhang, H., Chen, J., and Shen, S. Z.: Quantitative palaeogeographical reconstruction of the North China Block during the Carboniferous and Permian transition: Implications for coal accumulation and source rock development .Palaeogeogr Palaeocl, 640, 112102. https://doi.org/10.1016/j.palaeo.2024.112102, 2024.

Song, S.G., Niu, Y.L., Su, L., and Xia, X.H.: Tectonics of the North Qilian orogen, NW China: Gondwana Res, 23, 1378–1401, https://doi.org/10.1016/j.gr.2012.02.004. , 2013.

Song, D.F., Xiao, W., Collins, A. S., Glorie, S., Han, C., and Li, Y.: Final subduction processes of the Paleo-Asian Ocean in the Alxa Tectonic Belt (NW China): Constraints from field and chronological data of Permian arc-related volcano-sedimentary rocks. Tectonics, 37(6), 1658-1687. https://doi.org/10.1029/2017TC004919, 2018.

Song, D.F., Xiao, W.J., Windley, B.F., and Han, C.M.: Carboniferous to Early Triassic magmatism and accretion in Alxa (NW China): Implications for accretionary orogenesis of the southern Altaids. J Geol Soc London, 177(5), 997-1012. https://doi.org/10.1144/jgs2020-046, 2020.

Song, D.F., Xiao, W., Windley, B. F., and Han, C.: Provenance and tectonic setting of late Paleozoic sedimentary rocks from the Alxa Tectonic Belt (NW China): Implications for accretionary tectonics of the southern Central Asian Orogenic Belt. Geol Soc Am Bull, 133(1-2), 253-276. https://doi.org/10.1130/B35652.1, 2021.

Song, D.F., Mitchell, R.N., Xiao, W.J., Mao, Q.G., Wan, B., and Ao, S.J.: Andean-type orogenic plateau as a trigger for aridification in the arcs of northeast Pangaea. Commun Earth Environ 4: 306. https://doi.org/10.1038/s43247-023-00976-2, 2023.

Song, D.F., Xiao, W., Ao, S., Mao, Q., Wan, B., and Zeng, H.: Contemporaneous closure of the Paleo-Asian Ocean in the Middle-Late Triassic: A synthesis of new evidence and tectonic implications for the final assembly of Pangea. Earth-Sci Rev, 253, 104771. https://doi.org/10.1016/j.earscirev.2024.104771, 2024a.

Song, D.F., Xiao, W., Mao, Q., and Ao, S.: Tectonic evolution of the Alxa region, NW China: from a Precambrian continental ribbon to a Paleozoic–early Triassic accretionary orogen. J Geol Soc London, 182(2), jgs2023-222. https://doi.org/10.1144/jgs2023-222, 2024b.

Sun, B.N. and Xu, J.L.: Discovery of Plant Fossils in the Triassic Volcanic Rocks of the Baoji Mountain-Ciyao Mining Area. Journal of Lanzhou University (Natural Sciences), (04) (in Chinese with English abstract), 1988.

Sun, J.P., Dong, Y.P.: Cambrian tectonic evolution of the northwestern Ordos Terrane, North China: constraints of stratigraphy, sedimentology and zircon U-Pb geochronology. Int. J. Earth Sci. 108, 569–586. https://doi.org/10.1007/s00531-018-1669-8, 2018.

Sun, J.P., and Dong, Y.P.: Triassic tectonic interactions between the Alxa Massif and Ordos Basin: Evidence from integrated provenance analyses on sandstones, North China. J Asian Earth Sci, 169, 162–181. https://doi.org/10.1016/j.jseaes.2018.08.002, 2019.

Sun, J.P., and Dong, Y.: Stratigraphy and geochronology of Permo-Carboniferous strata in the Western North China Craton: Insights into the tectonic evolution of the southern Paleo-Asian Ocean. Gondwana Res, 88, 201-219. https://doi.org/10.1016/j.gr.2020.08.005, 2020.

https://doi.org/10.5194/egusphere-2026-4406
Preprint. Discussion started: 4 September 2026

Sun, J.P., and Dong, Y.: Foreland basin development in response to Proto-Tethyan Ocean closure, western North China Block. Geosphere, 20(3), 799-824. https://doi.org/10.1130/GES02725.1, 2024.

Sun, J., Dong, Y., Zhao, J., and Chen, Q.: Carboniferous to Triassic polyphase tectonic transition in the western North China craton: A retroarc basin response to termination of the middle segment of the Paleo-Asian Ocean. Geol Soc Am Bull, 136(9-10), 4149-4174. https://doi.org/10.1130/B37312.1, 2024.

Sundell, K. E., Eden, R., Styron, R. H., Villarreal, D. P., Usnayo, P., Saylor, J. E., and Carlotto, V.: Tectonic and climatic controls on late Cenozoic intra-arc basin development in the central Andes of southern Peru. Earth Planet Sc Lett, 666, 119487. https://doi.org/10.1016/j.epsl.2025.119487, 2025.

Tabor, N. J., and Poulsen, C. J.: Palaeoclimate across the Late Pennsylvanian–Early Permian tropical palaeolatitudes: a review of climate indicators, their distribution, and relation to palaeophysiographic climate factors. Palaeogeogr Palaeocl, 268(3-4), 293-310. https://doi.org/10.1016/j.palaeo.2008.03.052, 2008.

Tan, C., Ruan, Z., Yu, B., Li, Z., Liu, C., Zhao, L., and Jia, P.: Provenance and palaeogeomorphology study of the southwestern North China Craton during Middle-Late Triassic and its geological implication. Int Geol Rev, 64(13), 1781-1798. https://doi.org/10.1080/00206814.2021.1957028, 2022.

Tang, M., Ji, W. Q., Chu, X., Wu, A., and Chen, C.: Reconstructing crustal thickness evolution from europium anomalies in detrital zircons. Geology, 49(1), 76-80. https://doi.org/10.1130/G47745.1, 2021.

Tang, M., Chen, H., Lee, C. T. A., and Cao, W.: Subaerial crust emergence hindered by phase-driven lower crust densification on early Earth. Sci Adv, 10(37), eadq1952. https://doi.org/10.1126/sciadv.adq1952, 2024.

Tao, H., Cui, J., Sun, J., Ren, Z., Zhao, F., Su, S. and Song, H.: Late Carboniferous to Permian paleoclimatic and tectono-sedimentary evolution of the central Ordos Basin, western north China Block. Mar Petrol Geol, 173, 107287. https://doi.org/10.1016/j.marpetgeo.2025.107287, 2025.

Terrizzano, C. M., Morabito, E. G., Christl, M., Likerman, J., Tobal, J., Yamin, M., and Zech, R.: Climatic and Tectonic forcing on alluvial fans in the Southern Central Andes. Quaternary Sci Rev, 172, 131-141. https://doi.org/10.1016/j.quascirev.2017.08.002, 2017.

Tian, R.S., Xie, G.A., Zhang, J., Zhu, W.B., Qu, J.F., and Gao, S.: Sedimentary provenance and age of the Langshan Group in the northeastern Alxa Block: Implications for Neoproterozoic tectonic evolution. Int J Earth Sci, 108.5 (2019): 1705-1723. https://doi.org/10.1007/s00531-019-01731-9, 2019.

Tian, R.S., Xie, G.A., Zhu, W.B., Zhang, J., Gao, S., Zhang, B.H., Zhao, H., and Li, T.: Late Paleozoic tectonic evolution of the Paleo-Asian Ocean in the northern Alxa Block (NW China). Tectonics, 39(8), e2020TC006359. https://doi.org/10.1029/2020TC006359, 2020.

Tian, R.S., Xie, G.A., Zhu, W.B., and Gao, S.: Late Paleozoic magmatic flare-up in the Nuoergong-Langshan Belt, Alxa Block: Insights into tectonic evolution of the southern Paleo-Asian Ocean. Lithos. 398–399. https://doi.org/10.1016/j.lithos.2021.106310, 2021.

Tian, R.S., Wang, X., Ge, R., Zhu, W., and Xie, G.: Early to Middle Paleozoic magmatism and metamorphism in the Alxa Block and its northern margin: implications for the western extension of the Bainaimiao arc. Lithos, 440, 107041. https://doi.org/10.1016/j.lithos.2023.107041, 2023.

Tian, R.S., Yan, Z., and Xie, G.: Final subduction-closure process of the Paleo-Asian Ocean in the middle segments of the southern Central Asian Orogenic Belt: Constraints from Permian volcanic rocks and late Triassic mafic dike swarms. Lithos, 488, 107805. https://doi.org/10.1016/j.lithos.2024.107805, 2024.

Tong, Z. S.: On The relationship between carboniferous paleogeography and tectonics in the east part of the North Qilian Mountains. Gansu Geology, (02): 61-66(in Chinese with English abstract), 1993.

Tong, Z. S.: Basic features of Early Carboniferous sedimentary environment at Ciyao in Jingyuan County, Gansu. Journal of Lanzhou University (Natural Sciences), (01):104-110. (in Chinese with English abstract), 1994.

Tong, Z. S., and Hanye, L.: Characteristics of Carboniferous lithofacies and paleogeography in Eastern part of North Qilian. Acta Sedimentol. Sin., 20(1), 89-97. (in Chinese with English abstract), 1994.

Tong, J. N., Chu, D. L., Miao, X., Shu, W. C., Guo, W. W., Wu, Y. Y., and Yu, Y. Y.: Lithostratigraphic subdivision and correlation of the Triassic in China. Journal of Stratigraphy, 45(3), 340-3(in Chinese with English abstract). https://doi.org/10.19839/j.cnki.dcxzz.2021.0028, 2021.

Wang, Y., Li, J.Y., and Sun, G.H.: Postcollisional eastward extrusion and tectonic exhumation along the eastern Tianshan orogen, Central Asia: Constraints from dextral strike-slip motion and 40Ar/39Ar geochronological evidence. The Journal of Geology, 116(6), 599-618. https://doi.org/10.1086/591993, 2008.

Wang, B., Jahn, B.M., Lo, C.H., Shu, L.S., Wu, C.Y., Li, K.S., and Wang, F.: Structural analysis and 40Ar/39Ar thermochronology of Proterozoic rocks in Sjailimu area (NW China): Implication to polyphase tectonics of the north Chinese Tianshan. J Asian Earth Sci, 42(5), 839-853. https://doi.org/10.1016/j.jseaes.2011.07.022, 2011.

Wang, Z.N.: The geochronology, geochemistry and tectonic implications of mafic rocks in Helan Mountains. Northwest University, Xi'an, China, 1-71(in Chinese with English abstract), 2018.

Wang, Z.Z., Chen, X.H., Shao, Z.G., Li, B., Chen, H.X.,Ding, W.C., Zhang, Y.Y., and Wang, Y.C.: Geo-chronology, geochemistry and tectonic implications of early Carboniferous plutons in the southwestern Alxa Block. Geol Mag, 159(3), 372-388. https://doi.org/10.1017/S0016756821000984, 2022a.

Wang, Y.D., Yang, S.L., Zhang, S.H., Huang, X.F., Sun, M.M., and Ding, Z.L.: Early–middle Permian drying in the North China Block induced by large igneous provinces. Palaeogeogr Palaeocl, 592. https://doi.org/10.1016/j.palaeo.2022.110922, 2022b.

Wang, Z.Z., Chen, X.H., Ding, W.D., Li, B., Zhang, Y.P., Shao, Z.G., and Xu, S.L.: Late Carboniferous extension-related magmatism in the southwestern Alxa block of NW China: Geochronology, geochemistry, and tectonic implications. Int Geol Rev, 65(9),1558-1585. https://doi.org/10.1080/00206814.2022.2098833, 2023a.

Wang, Y., Yang, J., Henderson, C. M., Yuan, D., Ma, R., and Liu, J.: Carboniferous-Permian high-resolution conodont biostratigraphy and paleoclimate change in North China. Palaeogeogr Palaeocl, 629, 111782. https://doi.org/10.1016/j.palaeo.2023.111782, 2023b.

Wei, X.Y., Lu, J.C., Wei, J.S., Li, Y.H.: Petroleum geological conditions and petroleum-bearing prospect of Carboniferous-Permian strata in Hexi Corridor region. Geological Bulletin of China, 30(6): 865-878. (in Chinese with English abstract), 2011.

Wu, C., Yin, A., Zuza, A.V., Zhang, J.Y., Liu, W.C., and Ding, L.: Pre-Cenozoic geologic history of the central and northern Tibetan Plateau and the role of Wilson cycles in constructing the Tethyan orogenic system. Lithosphere, 8. 254-292. https://doi.org/10.1130/L494.1, 2016.

Wu, Q., Ramezani, J., Zhang, H., Wang, J., Zeng, F.G., Zhang, Y.C., Liu, F., Chen, J., Cai, Y.F., Hou, Z.S., Liu, C., Yang, W., Henderson, C.M., and Shen, S.Z.: High-precision U-Pb age constraints on the Permian floral turnovers, paleoclimate change, and tectonics of the North China block. Geology, 49. 677-681. https://doi.org/10.1130/G48051.1, 2021.

Wu, Q., Zhang, H., Ramezani, J., Zhang, F. F., Erwin, D. H., Feng, Z., and Shen, S. Z.: The terrestrial end-Permian mass extinction in the paleotropics postdates the marine extinction. Sci Adv, 10(5), eadi7284. https://doi.org/10.1126/sciadv.adi7284, 2024.

Xiao, W., Windley, B. F., Hao, J., and Zhai, M.: Accretion leading to collision and the Permian Solonker suture, Inner Mongolia, China: Termination of the central Asian orogenic belt. Tectonics, 22(6). https://doi.org/10.1029/2002TC001484, 2003.

Xiao, W.J., Windley, B.F., Yong, Y., Yan, Z., Yuan, C., Liu, C.Z., and Li, J.L.: Early Paleozoic to Devonian multiple-accretionary model for the Qilian Shan, NW China, J Asian Earth Sci, 35, 323–333. https://doi.org/10.1016/j.jseaes.2008.10.001, 2009.

Xiao, W., Windley, B. F., Sun, S., Li, J., Huang, B., Han, C., and Chen, H.: A tale of amalgamation of three Permo-Triassic collage systems in Central Asia: Oroclines, sutures, and terminal accretion. Annu Rev Earth Pl Sc, 43(1), 477-507. https://doi.org/10.1146/annurev-earth-060614-105254, 2015.

Xiao, W., Song, D., Windley, B. F., Li, J., Han, C., Wan, B., and Zhang, Z.: Accretionary processes and metallogenesis of the Central Asian Orogenic Belt: Advances and perspectives. Sci China Earth Sci, 63(3), 329-361. https://doi.org/10.1007/s11430-019-9524-6, 2020.

Xin, B. S., Yang, H., Fu, J. H., Wang, D. Y., Yao, J. L., Zhang, Y., and Zuo, B.: SHRIMP U-Pb zircon age and its stratigraphic significance of tuff at the bottom of the Upper Triassic Nanyinger Group, Mount Baoji Area, Jingyuan County, Gansu Province. Geological Review, 59(2), 267-273 (in Chinese with English abstract), 2013a.

Xin, B., Yang, H., Wang, D., Fu, J., Yao, J., Luo, A., & Zhang, Y.: SHRIMP U-Pb age and its stratigraphic significance of tuff at the Baojishan Area, Jingyuan County, Gansu Province. Advances in Earth Science, 28(9), 1043-1048 (in Chinese with English abstract), 2013b.

Xu, J.L., Sun, B.M., Wang, J., Liu, H.Q., X, A.M.: Problems on Succession of Carboniferous-Permian Systems at Dahuanggou Valley along Northern Slope of Western Qilian Mountains. Journal of Lanzhou University (Natural Sciences), (04):2 68-273 (in Chinese with English abstract), 1993.

Xu, Y.J., Du, Y.S., Cawood, P.A., Guo, H., Huang, H., and An, Z.H.: Detrital zircon record of continental collision: Assembly of the Qilian Orogen, China. Sediment Geol, 230, 35-45. https://doi.org/10.1016/j.sedgeo.2010.06.020, 2010.

Xu, Y.J., Du, Y.S., and Yang, J.H.: Tectonic evolution of the North Qilian orogenic belt from the Late Ordovician to Devonian: Evidence from detrital zircon geochronology. J Earth Sci-China, 5, 31-43 (in Chinese with English abstract), 2013.

Yan, C.F.: Lithofacies Paleogeography of the Carboniferous in the East of North Qilian Mountains. Acta Sedimentol. Sin. 26(2): 193-201. (in Chinese with English abstract), 2008.

Yan, Y., Peng, R., Chen, S., Li, S.: Discovery and geological significance of an Indosinian (ca. 244 Ma) metamorphic event in the Langshan area, western Inner Mongolia, China: new evidence from zircon LA-ICP-MS U-Pb dating. J. Earth Sci. 33 (4), 993-1006. https://doi.org/10.1007/s12583-020-1112-5, 2022.

Yang, J.H., Du, Y.S., Cawood, P.A., and Xu, Y.J.: Silurian collisional suturing onto the southern margin of the North China craton: Detrital zircon geochronology constraints from the Qilian Orogen. Sediment Geol, 220, 95-104. https://doi.org/10.1016/j.sedgeo.2009.07.001, 2009.

Yang, J.H., Du, Y.S., Cawood, P.A., and Xu, Y.J.: Modal and geochemical compositions of the Lower Silurian clastic rocks in North Qilian, NW China: Implications for provenance, chemical weathering, and tectonic setting. J Sediment Res, 82, 92-103. https://doi.org/10.2110/jsr.2012.6, 2012.

Yang, J.H., Cawood, P. A., Du, Y., Feng, B., and Yan, J.: Global continental weathering trends across the Early Permian glacial to postglacial transition: Correlating high-and low-paleolatitude sedimentary records. Geology, 42(10), 835-838. https://doi.org/10.1130/G35892.1, 2014.

Yang, J.H., Cawood, P. A., Montañez, I. P., Condon, D. J., Du, Y., Yan, J. X. and Yuan, D.: Enhanced continental weathering and large igneous province induced climate warming at the Permo-Carboniferous transition. Earth Planet Sc Lett, 534, 116074. https://doi.org/10.1016/j.epsl.2020.116074, 2020.

Yang, X., Dong, Y., Sun, J., Feng, Y., Xiang, L., Li, M., and Wang, Z.: The Triassic tectonic transition of the Northwestern margin of Ordos Basin, North China Craton. Int Geol Rev, 67(11), 1486-1507. https://doi.org/10.1080/00206814.2025.2456984, 2025a.

Yang, C., Sun, J., Li, Z., Qi, Y., Ye, K., Zhang, J., and Wang, Z.: Carboniferous-Permian provenance shift in the southeastern Ordos Basin: Tracing early-stage uplift-erosion history of the western Qinling-Dabie orogen. Acta Geochim, 1-17. https://doi.org/10.1007/s11631-025-00765-y, 2025b.

Zhang, J., Ma, Z. J., and Ren, W. J.: Rediscussion on natures of extension in Helanshan region before Cenozoic era. Acta Petrolei Sinica, 25(6), 8 (in Chinese with English abstract), 2004.

Zhang, J.X., and Gong, J.H.: Revisiting the nature and affinity of the Alxa block: Acta Petrologica Sinica (YanShi Xuebao), 34(4). 940–962 (in Chinese with English abstract), 2018.

https://doi.org/10.5194/egusphere-2026-4406
Preprint. Discussion started: 4 September 2026

Zhang, J., Li, J.Y., Xiao, W.X., Wang, Y.N., and Qi, W.H.: Kinematics and geochronology of multistage ductile deformation along the eastern Alxa block, NW China: New constraints on the relationship between the North China plate and the Alxa block. J Struct Geol, 57. 38-57. https://doi.org/10.1016/j.jsg.2013.10.002, 2013.

Zhang, S.H., Zhao, Y., Ye, H., Liu, J.M., and Hu, Z.C.: Origin and evolution of the Bainaimiao arc belt: Im plications for crustal growth in the southern Central Asian orogenic belt: Geol Soc Am Bull, 126, 1275–1300, https://doi .org /10 .1130 /B31042 .1, 2014.

Zhang, J.J., Wang, T., Zhang, L., Tong, Y., Zhang, Z.C., Shi, X.J., Guo, L., Huang, H., Yang, Q.D., Huang, W., Zhao, J.X., Ye, K., and Hou, J.Y.: Tracking deep crust by zircon xenocrysts within igneous rocks from the northern Alxa, China: Constraints on the southern boundary of the Central Asian Orogenic Belt. J Asian Earth Sci, 108. 150-169. https://doi.org/10.1016/j.jseaes.2015.04.019, 2015.

Zhang, B.H., Zhang, J., Zhao, H., Nie, F.J., Wang, Y.N., and Zhang, Y.P.: Tectonic evolution of the western Ordos Basin during the Palaeozoic-Mesozoic time as constrained by detrital zircon ages. Int Geol Rev, 61. 461-480. https://doi.org/10.1080/00206814.2018.1431963, 2019.

Zhang, J., Cunningham, D., Qu, J., Zhang, B., Li, J., Zhao, H., and Zhang, Y.: Poly-phase structural evolution of the northeastern Alxa Block, China: Constraining the Paleozoic-Recent history of the southern central Asian Orogenic belt. Gondwana Res, 105, 25-50. https://doi.org/10.1016/j.gr.2021.12.007, 2022.

Zhang, J.X., Yu, S.Y., Li, Y.S., and Mao, X.H.: Proto-Tethys orogenic system in the northern Qinghai-Tibet Plateau: Resubdivision of lithotectonic units in Qilian-North Qaidam and discussion on several controversial scientific issues. Acta Petrol Sin, 39(12): 3507-3532 https://doi.org/10.18654/1000-0569/2023.12.01, 2023.

Zhang, T., Chen, R., Wang, F., Hu, J., Zhang, M., Li, Q. and Liu, L.: Provenance of the Upper Carboniferous Yanghugou Formation in the Western Margin of the Ordos Basin, China. Constraints on Paleogeography and Basin Development. Minerals, 14(1), 78. https://doi.org/10.3390/min14010078, 2024.

Zhao, G.C., Cawood, P.A., Wilde, S.A., Sun, M., Zhang, J., He, Y.H., and Yin, C.Q.: Amalgamation of the North China Craton: Key issues and discussion. Precambrian Res, 222–223. 55–76. https://doi.org/10.1016/j.precamres.2012.09.016, 2012.

Zhao, G., Wang, Y., Huang, B., Dong, Y., Li, S., Zhang, G., and Yu, S.: Geological reconstructions of the East Asian blocks: From the breakup of Rodinia to the assembly of Pangea. Earth-Sci Rev, 186, 262-286. https://doi.org/10.1016/j.earscirev.2018.10.003, 2018.

Zhao, J., Zhou, Y., Wang, K., Li, X., Ma, Z., Ruan, Z., and Xue, R.: Provenance and paleogeography of Carboniferous–Permian strata in the Bayanhot Basin: Constraints from sedimentary records and detrital zircon geochronology. Geosci Front, 12(3), 101088. https://doi.org/10.1016/j.gsf.2020.09.017, 2021.

Zheng, R. G. and Zhang, J.: Tectonic switching during Carboniferous-Early Triassic within the southern Alxa. Geological Bulletin of China, 43(12): 2190-2203 (in Chinese with English abstract). https://doi.org/10.12097/gbc.2024.08.028, 2024.

https://doi.org/10.5194/egusphere-2026-4406
Preprint. Discussion started: 4 September 2026

Zheng, R. G., Wu, T. R., Zhang, W., Xu, C., Meng, Q. R., and Zhang, Z. Y.: Late Paleozoic subduction system in the northern margin of the Alxa block, Altaids: Geochronological and geochemical evidences from ophiolites. Gondwana Res, 25(2). 842–858 https://doi.org/10.1016/j.gr.2013.05.011, 2014.

Zheng, R.G., Li, J.Y., Xiao, W.J., and Wang, L.J.: A new ophiolitic mélange containing boninitic blocks in Alxa region: Implications for Permian subduction events in southern CAOB. Geosci Front, 9. 1355-1367. https://doi.org/10.1016/j.gsf.2018.02.014, 2018.

Zheng, R.G., Li, J.Y., and Zhang, J.: Juvenile hafnium isotopic compositions recording a late Carboniferous-Early Triassic retreating subduction in the southern Central Asian Orogenic Belt: A case study from the southern Alxa. Geol Soc Am Bull, 134. 1375-1396. https://doi.org/10.1130/B35991.1, 2022.

Zuza, A.V., Wu, C., Reith, R.C., Yin, A., Li, J.H., Zhang, J.Y., Zhang, Y.X., Wu, L., and Liu, W.C.: Tectonic evolution of the Qilian Shan: An early Paleozoic orogeny reactivated in the Cenozoic. Geol Soc Am Bull, 130. 881-925.https://doi.org/10.1130/B31721.1, 2018.